Analysis and control of a laser tracking system

Theunissen, H.W.H.

Award date:
1999

Eindhoven University of Technology
Department of Electrical Engineering
Measurement and Control Group

Analysis and control of a laser tracking system

by

H.W.H. Theunissen

Master of Science Thesis
carried out from April 1998 to February 1999
commissioned by Prof. Dr. Ir. P. P.J. van den Bosch
under supervision of Dr. Ir. A.A.H. Damen
date: 3 February 1999

Abstract

In the measurement and control group a laser tracking system is being developed to measure or calibrate the tool centre point of a robot. A laser beam is pointed at the centre of a mirror in an air bearing seat and deflected to a retro-reflector, which is attached to the end of the robot arm. The returned laser beam is split in two by a beam-splitter. One part passes the beam-splitter and is received in a laser interferometer, which measures the distance the laser beam has passed. The other part of the laser beam is deflected to a position sensitive device. This device is used to control the tilting of the mirror such that the laser beam hits the retro-reflector exactly in its centre. By measuring the two angles of the mirror and the length the laser beam has followed the position of the tool centre point can be calculated.

For this final thesis first of all the accuracy of the laser tracking system has been analysed theoretically. The effects of several kinds of inaccuracies have been calculated in a two-dimensional space. The inaccuracies are divided into inaccuracies caused by several kinds of displacements and inaccuracies of optical components and external influences. With displacements are meant movements of the mirror in its bearing seat and wrong alignments of the optical components. For all the inaccuracies caused by displacements the deviation of the distance the laser beam travels according to the ideal situation has been calculated. The same has been done for one angle of the mirror. From these calculations may be concluded that the deviations according to the ideal situation are acceptable.

From the accuracy analysis can be concluded that it is important to control the air gap of the mirror's semi sphere in its bearing seat. The air gap should stay on a constant value. Two H_∞ controllers have been designed. One based on a seventh order model of the process and one based on an approximated third order model of the process. The calculated controllers have been tested in Simulink. The simulations showed that the actuator does not saturate and that the air gap varies with an acceptable value for a certain bandwidth. For testing the controller on the real system, the controller has been implemented in a dSPACE system. The controller based on the third order model performed like the simulations showed. The controller based on the seventh order model could not be implemented because of a limited sample frequency of the dSPACE system. To control the two angles of the mirror, two angle controllers have been designed. Again there is chosen for H_∞ controllers. These controllers have also been tested first in Simulink before implementation on the real system.

Samenvatting

In de leerstoel meten en regelen een lasermeetsysteem is in ontwikkeling voor het meten of kalibreren van de eindtip van een robot. Een laserbundel wordt gericht op het midden van een luchtgelagerd spiegeltje en gereflecteerd naar een retro-reflector. De terugkomende laserbundel wordt in tweeën gesplitst door een halfdoorlatende spiegel. Een deel van de laserbundel passeert de halfdoorlatende spiegel en komt terecht in een laserinterferometer, die de afgelegde weg van de laserbundel meet. Het andere deel van de laserbundel wordt gereflecteerd naar een positie gevoelig element. Dit element wordt gebruikt om de bewegingen van het spiegeltje te kunnen regelen zodat de laserbundel precies op het midden van de retro-reflector wordt gericht. Door de twee hoeken van het spiegeltje te meten en de afgelegde weg van de laserbundel kan de positie van de eindtip berekend worden.

In het kader van het afstudeerwerk is ten eerste de nauwkeurigheid van het lasermeetsysteem theoretisch geanalyseerd. De invloeden van verschillende onnauwkeurigheden zijn berekend in een twee-dimensionale omgeving. De onnauwkeurigheden zijn verdeeeld in onnauwkeurigheden veroorzaakt door verschillende soorten verplaatsingen en onnauwkeurigheden van optische componenten en externe invloeden. Met verplaatsingen worden bedoeld bewegingen van het spiegeltje in zijn lager en verkeerde uitlijningen van de optische elementen. Voor alle onnauwkeurigheden veroorzaakt door verplaatsingen is de afwijking berekend van de afgelegde weg van de laserbundel ten opzichte van de ideale situatie. Hetzelfde is gedaan voor één hoek van het spiegeltje. Uit deze berekeningen mag geconcludeerd worden dat de afwijkingen ten opzichte van de ideale situatie acceptabel zijn.

Uit de nauwkeurigheidsanalyse kan geconcludeerd worden dat het belangrijk is om de luchtspleet van de halve bolvormige spiegel in zijn luchtlager te regelen. De luchtspleet moet op een constante waarde worden gehouden. Er zijn twee H_∞ regelaars ontworpen. De ene is gebaseerd op een zevende orde model van het proces en de andere is gebaseerd op een benaderd derde orde model van het proces. De berekende regelaars zijn getest in Simulink. Uit de simulaties volgden dat de actuator niet overstuurd raakte en dat de luchtspleet varieerde binnen acceptabele waarden voor een bepaalde bandbreedte. Om de regelaar te testen op het werkelijke systeem is de regelaar geïmplementeerd in een dSPACE-systeem. De regelaar die gebaseerd is op het derde orde model werkte zoals de simulaties voorspelden. De regelaar die gebaseerd is op het zevende orde model kon niet geïmplementeerd worden in verband met een gelimiteerde samplefrequentie van het dSPACE-systeem.
Voor het regelen van de twee hoeken van het spiegeltje zijn twee regelaars ontworpen. Er is weer gekozen voor H_∞ regelaars. Ook deze regelaars zijn eerst getest in Simulink alvorens ze geïmplementeerd zijn in het werkelijke systeem.

Table of contents

1. Introduction

1.1 The laser tracking system

The Measurement and Control group of the Department of Electrical Engineering at Eindhoven University of Technology is doing research on modelling, identification and control of processes.
One of the laboratory processes is a laser tracking system. By means of a revolving mirror in an air-bearing seat, a reflector can be followed by a laser beam. The reflector is attached to the end of the robot arm. In this way it is possible to measure or calibrate the TCP (Tool Centre Point) of a robot. In Figure 1.1 a schematic top view of the laser tracking system is shown.

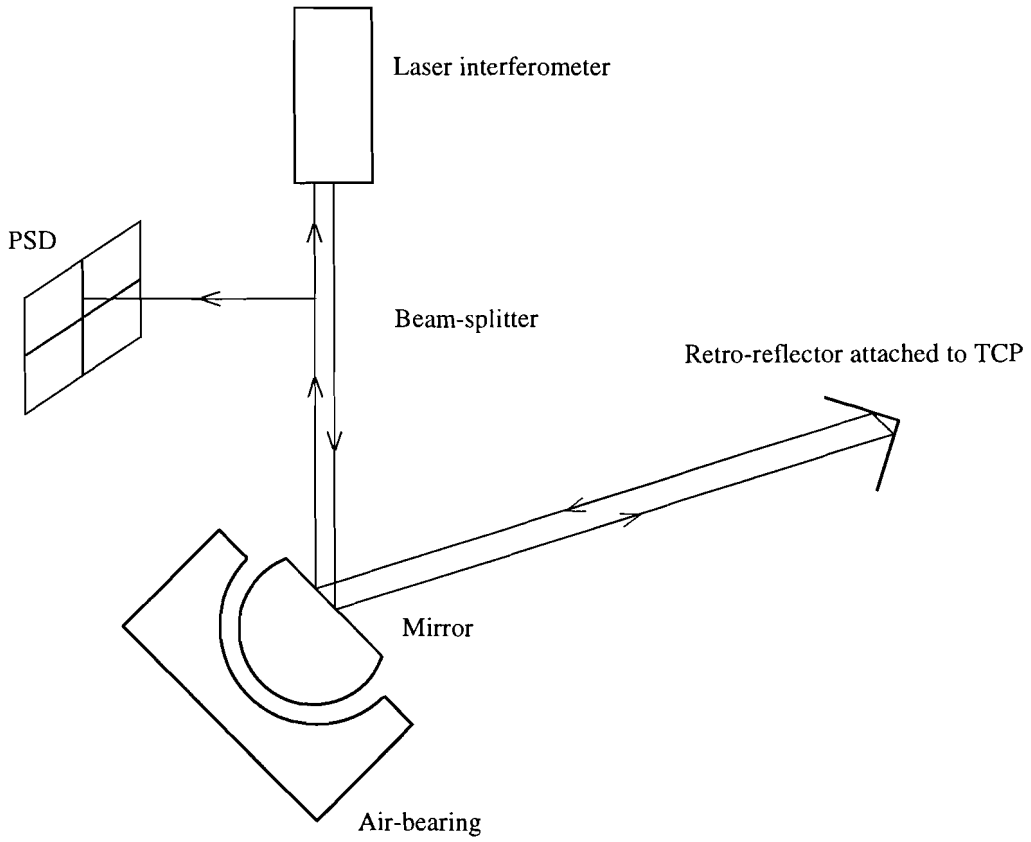

Figure 1.1: Top view of the laser tracking system

The reflector is a retro-reflector it returns the laser beam parallel to the incoming beam, independent of the angle of incidence. The laser beam is reflected by the mirror and split in two by a beam-splitter. One part passes the beam-splitter and is received in the interferometer. This device measures the length the laser beam has travelled. The other part of the laser beam is deflected on a PSD (Position Sensitive Device), which measures the deviation of the reflected laser beam from the reflector's centre.

Two angle controllers generate new set points for the mirror so that the laser beam finally is pointed at the centre of the reflector. The sensors coupled to the rotatable mirror measures the angles of the mirror. With these two angles and the length of the laser beam the position of the TCP can be calculated.

1.2 Accuracy analysis

For further research it is important to determine the final accuracy of the laser tracking system. The accuracy depends on the performance of the various components. The sensitivity of the final tracking error for various error sources will be analysed.

The following effects will be studied:
- A "side slip" of the semi sphere.
- An air gap variation of the semi sphere in its bearing seat.
- Wrong alignment of the PSD.
- The laser beam does not point at the centre of the mirror.

Besides these error sources there are also inaccuracies from the optical components and the sensitivity of the sensors. And finally external influences, such as temperature variations and air composition variations, will make the system less accurate. The aimed performance for the system is an accuracy of 100 μm at a distance of 2 to 10 meters.

1.3 Various modes

The laser tracking system operates in various modes:
- Scanning mode.
- Tracking mode.
- Measuring mode.

- Scanning mode

The system first operates in the scanning mode. In this mode the laser beam moves in a pattern across the room, searching for the retro-reflector, by tilting the mirror in different directions. When the laser beam hits the retro-reflector the PSD detects an incoming beam and the system will be switched to the tracking mode.

- Tracking mode

The tracking mode is the most important mode and is already explained in section 1.1.

In this mode the system should meet two goals:
1. The system should measure the TCP of the robot with a high accuracy.
2. The system should follow the retro-reflector even when the robot is moving at a high speed.

Contrary to the scanning mode, in the tracking mode the signal of the PSD is available for controlling the mirror-angles.

- Measurement mode

In the measurement mode the two angles of the mirror and the travelled distance of the laser beam will be measured. The two angles are measured with the angle sensors and the distance is measured with a laser interferometer. With these two angles and the distance the position of the TCP of the robot can be computed.

1.4 Controller design

Two controllers should be designed:
1. An air gap controller for keeping the air gap height on a constant value.
2. Two angle controllers for controlling the two angles of the mirror.

The air gap controller is active in all the various modes. This controller should keep the air gap on a constant value.
The angle controllers control the two angles of the mirror with the available information from the PSD. The output of the PSD is an indication of the difference of the laser beam from the retro-reflector's centre. An overview of the controlling system is presented by a block scheme of Figure 1.2.

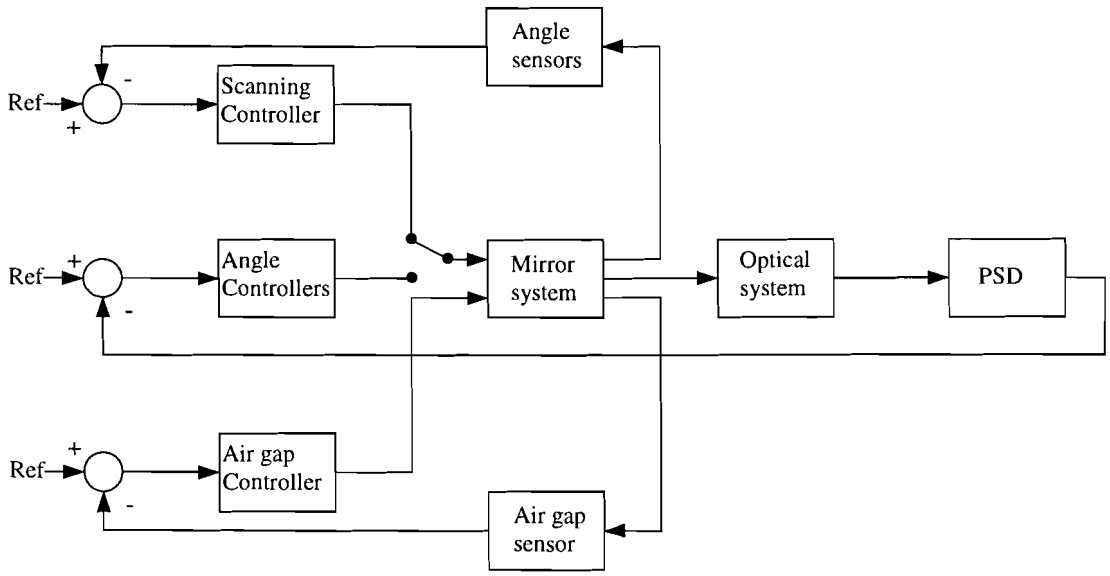

Figure 1.2: Block scheme of the controlling of the laser tracking system

There is chosen for robust controllers, to control the laser tracking system. When using a robust controller you have to make a trade off between robustness and performance. With a robust controller it is possible to define and quantify the control aims very clearly by weighting them relatively.

2. System description

The system consists of a reflective mirror in an air bearing seat, optical instruments, sensors and actuators. The components of the system are described in this chapter.

2.1 Mechanical description of the system

The mirror consists of a steel semi sphere, which can rotate on an air bearing. The air bearing gives rise to a very low friction.
Three electromagnetic actuators turn the semi sphere via strings, see Figure 2.1. These very stiff strings are connected to a plastic ring that is placed on the top of the mirror's surface.

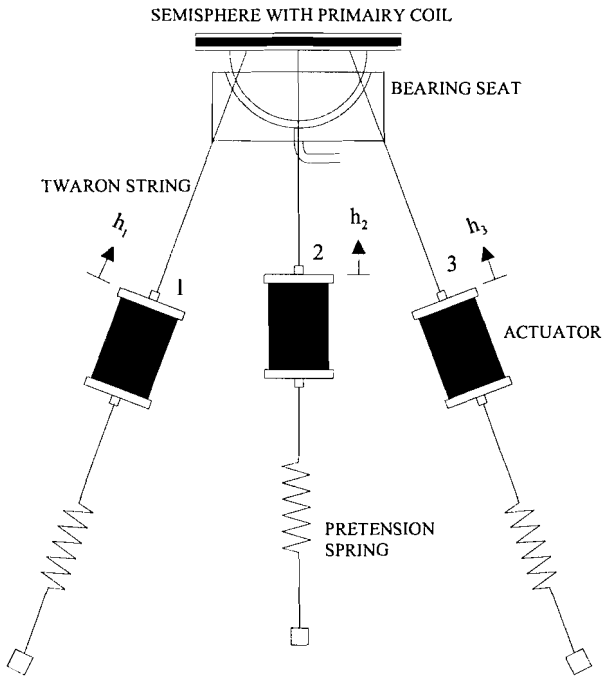

Figure 2.1: Mechanics of the mirror system

By pulling and revealing the strings the orientation of the mirror can be controlled. The actuators also control the air gap height, when all three strings are pulled or revealed at the same time. The pretension springs prevent the mirror from falling out of its seat.

2.2 The laser interferometer

The laser selected is a He-Ne-laser with a beam diameter of 2 mm and a wavelength of 632.5 nm. The purpose of the laser interferometer is to measure the distance of the end-effector from the laser tracking system.

2.3 The retro-reflector

The retro-reflector, which is used, is called a "corner cube" retro-reflector.
This retro-reflector consists of three mutually orthogonal, flat mirrors intersecting at a point (R), which is called the "centre" of the reflector. Ideal retro-reflectors have the properties that, regardless of the reflector orientation, an incident beam and the reflected beam are parallel and that the centre point is always exactly in the middle between the incident and the reflected beam. These properties are shown in Figure 2.2 for the two-dimensional case, but also hold for the three-dimensional case.

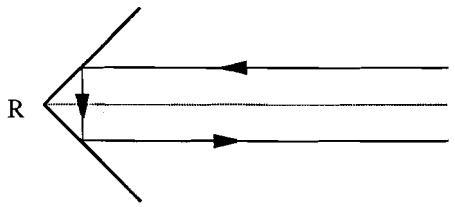

Figure 2.2: Retro-reflector principle

2.4 The beam-splitter

The beam-splitter is needed to split the reflected laser beam, so that one part is deflected to the PSD. The other part passes the beam-splitter and is received by the laser interferometer.

2.5 The PSD

To measure the error in tracking of the target with the laser beam a Position Sensitive Device is used. The PSD consists of two parts. The actual sensor that detects the light and generates an output signal and the electronics that processes these signals. In Figure 2.3 a two-dimensional structure of a PSD and its equivalent circuit is shown.

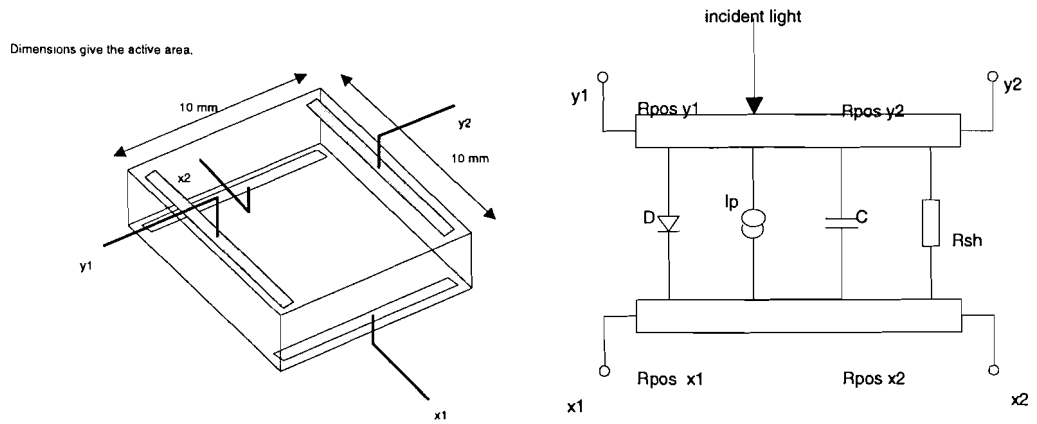

Figure 2.3: Two-dimensional structure and its equivalent circuit

When the centre point of the PSD is set at the original point, the position of the light spot on the PSD can be found by the following formulas:

$$x = \frac{L}{2} \cdot \frac{X_2 - X_1}{X_1 + X_2} \qquad y = \frac{L}{2} \cdot \frac{Y_2 - Y_1}{Y_1 + Y_2}$$

Where X_1, X_2, Y_1 and Y_2 represent the output signals (photo current) of each electrode and x and y are the co-ordinate positions of the light spot. L represents the dimensions of the active area of the PSD, in our case holds L = 10 mm.

2.6 The sensors

The tracking system uses two different kinds of sensors. One sensor-type is used for measuring the air gap height. The other type measures the angles of the mirror.

2.6.1 The air gap sensor

For stabilisation of the vertical movement of the mirror in its bearing seat, the height of the mirror in its semi sphere is measured, see also Figure 2.4. The mirror and the bearing seat are made of metal. So the measuring can be done contact less by measuring the electrical capacitance of the air gap (δ) between the semi sphere and the bearing seat.

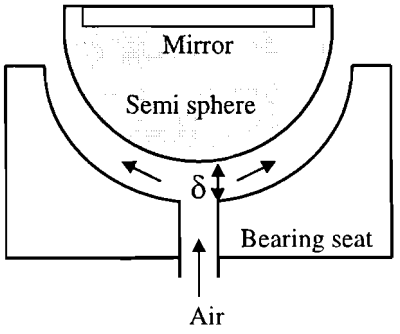

Figure 2.4: Air gap height δ

2.6.2 The angle sensors

For measuring the angles of the mirror, two sets of inductively coupled coils are used. In Figure 2.5 is shown that the sensor-system consists of one primary and two secondary coils.

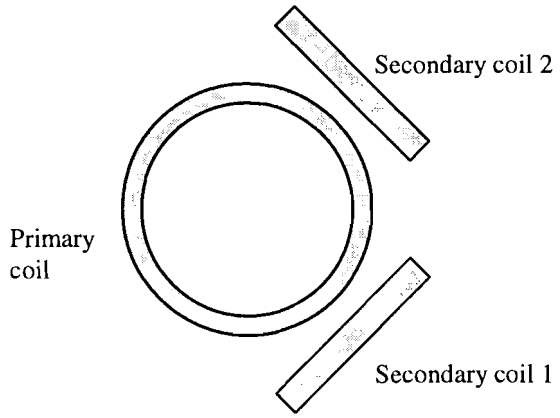

Figure 2.5: The angle sensors

The primary coil is energised with an external sine wave.
The current through the primary coil causes a flux through both the secondary coils.
The flux depends on the orientation of the mirror. This is shown for one secondary coil in Figure 2.6.

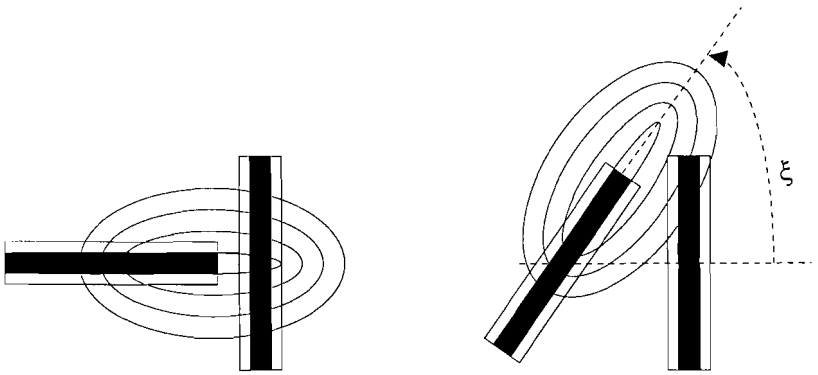

Figure 2.6: Flux through the secondary coils

When the mirror is positioned in its equilibrium, the resulting flux through the secondary coils is zero. When the mirror rotates, the resulting flux through the secondary coils is not zero, which causes a current through the secondary coils.
The current through the secondary coils is therefore related to the angles of the mirror.

2.7 The actuators

The laser tacking system uses three electromagnetic actuators, based on the principle of a loudspeaker. A coil moves in a magnetic field as a result of a current through it, see Figure 2.7.

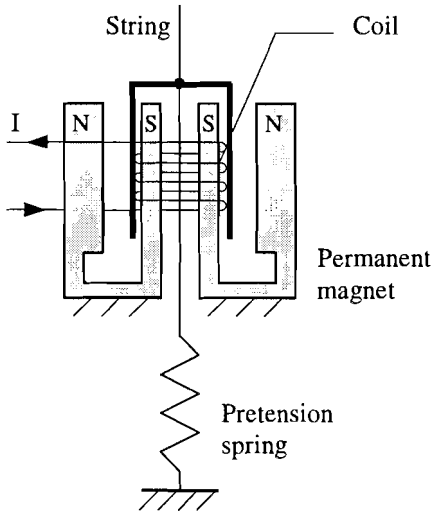

Figure 2.7: Principle of the actuators

The permanent magnet produces a homogeneous magnetic field (B). In this field the coil can move up and down. This movement is induced by a Lorentz force (F), which results from a current (I) through the coil. The direction of the Lorentz force is related to the direction of B and I as in Figure 2.8 where one winding is drawn.

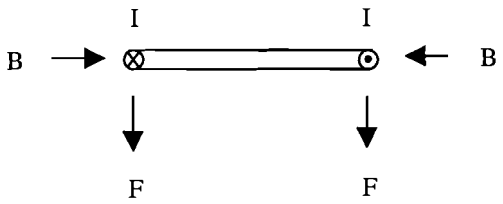

Figure 2.8: Movement of the actuators

The actuator coil moves also in an air bearing, so the friction associated with this movement is very low.

3. The accuracy of the laser tracking system in 2-D

The overall accuracy of the system depends on several kinds of inaccuracies, which can be divided into:

- Inaccuracies caused by several kinds of displacements:
  - A "side slip" of the semi sphere.
  - An air gap variation of the semi sphere in its bearing seat.
  - Wrong alignment of the PSD.
  - The laser beam does not point at the centre of the mirror.
- Inaccuracies of the optical components.
- Inaccuracies caused by external influences.
- Sensitivity of the sensors.

The sensitivity of the laser tacking system for various displacements is computed in a two-dimensional space.

For the ideal situation holds:

- The air pressure holds the semi sphere right in the centre of the bearing seat; this means that there is no "side slip".
- The air gap controller takes care for a constant air gap.
- The PSD and beam-splitter are aligned corresponding to the mirror and the laser.
- The laser is aligned corresponding to the mirror.
- There are no external influences, such as temperature variations, air composition variations and mechanical vibrations.
- The resolutions of the sensors are low enough for measuring the air gap height and the angles.

3.1 Effect of a "side slip" of the semi sphere

With the "side slip" of the semi sphere is meant the displacement of the semi sphere in its bearing seat, along the nominal position of the mirror surface, see Figure 3.1. In the ideal situation this movement does not appear, because the air pressure should hold the semi sphere exactly in the middle of the air bearing.

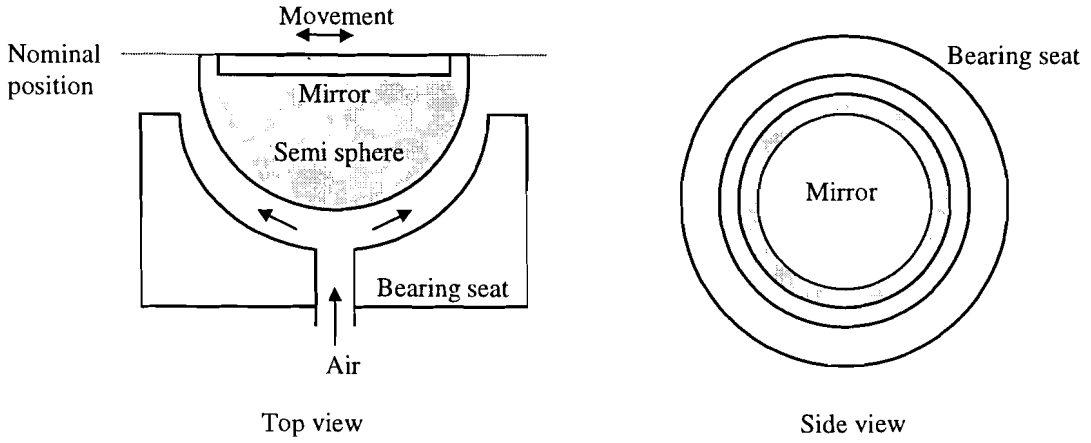

Figure 3.1: Top and side view of the semi sphere in its bearing seat

For calculating this effect on the accuracy of the system it is assumed that the laser beam hits the centre of the retro-reflector. To give an impression of this effect, see Figure 3.2, where a two-dimensional schematic view is shown of a "side slip".

The accuracy of the system is influenced in two ways:

1. ***Wrong distance measurement:*** *The distance the laser beam will travel during measuring is different by a "side slip" of the semi sphere, because the laser travels another path.*
2. ***Wrong angle measurement:*** *Because of the "side slip" the laser beam will be deflected differently. So the angle of the mirror will be changed to let the laser beam point again at the centre of the retro-reflector.*

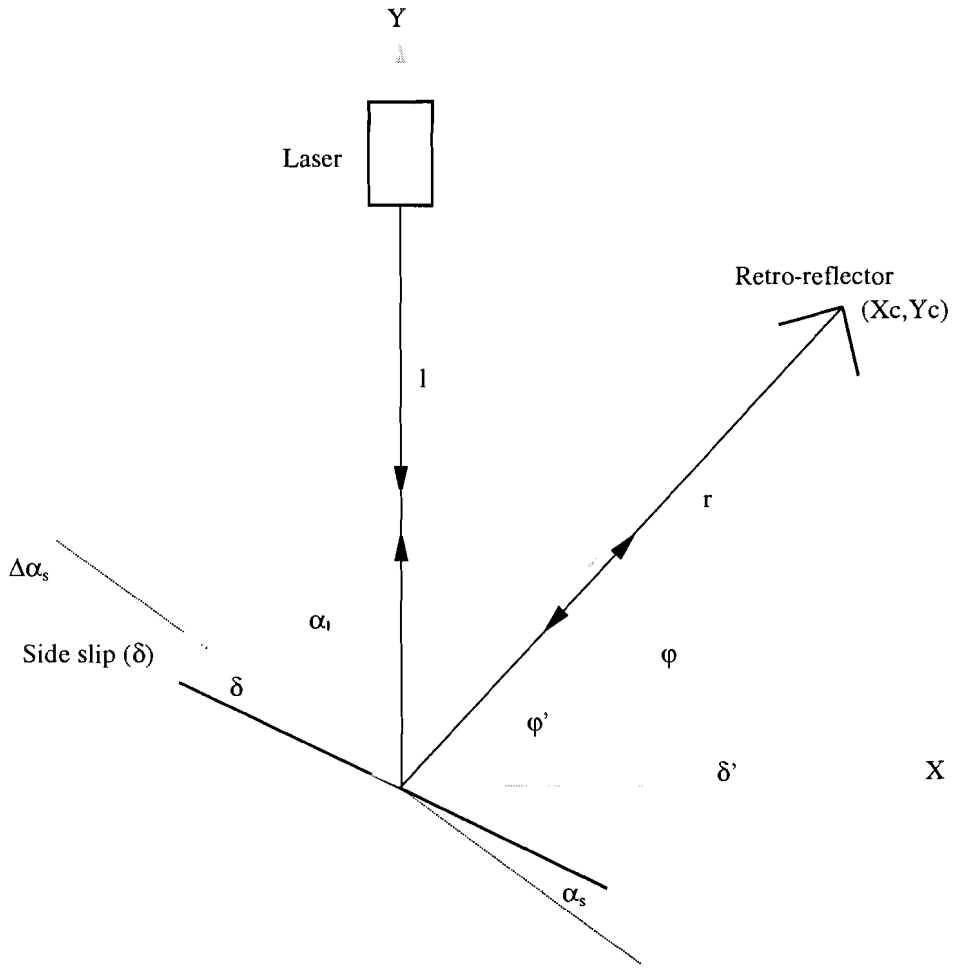

Figure 3.2: "Side slip" of the semi sphere

Nominal position of the mirror

Position of the mirror before side slip

Position of the mirror after side slip of distance δ, but before the corrected mirror-angle

Position of the mirror after side slip and with corrected mirror-angle

1. Wrong distance measurement

Computation of the deviation of the length the laser beam will travel by a "side slip" of the semi sphere

For explanations of used symbols, see Appendix A: "Explanations of used symbols in computations."

Position retro-reflector: $Xc = r\cos\varphi$

$Yc = r\sin\varphi$

$\varphi = 2(\alpha_s + \alpha_l) - \frac{\pi}{2}$

"Side slip": δ

Effect of the "side slip" in the Y-direction:

$$\delta' = \frac{\delta \sin\alpha_s}{\sin(\pi - \alpha_l - \alpha_s)} \tag{3.1}$$

Travelled distance of the laser beam, without a "side slip":

$$L_1 = 2(l + r)$$

Travelled distance of the laser beam, by a "side slip":

$$L_2 = 2\{\ l - \delta' + \sqrt{Xc^2 + \{\ Yc - \delta'\ \}^2}\ \}$$

Deviation: $$D = L_2 - L_1 = 2\{\ -\delta' + \sqrt{Xc^2 + \{\ Yc - \delta'\ \}^2} - r\ \}$$

Deviation in first order approximation:

$$D \approx -2\delta'\{\ 1 + \sin\varphi\ \} \tag{3.2}$$

So the deviation is independent of the measuring distance (r), if second and higher order terms are neglected. More details for this approximation are given in Appendix B: "The proof of the independence of the measuring distance on the length the laser beam travels."

In Figure 3.3 the deviation (in mm) of the length the laser beam travels by a "side slip" is plotted. The assuming value of δ is chosen 1 μm. From equation (3.1) and (3.2) may be concluded that the behaviour of the deviation is linear in δ.

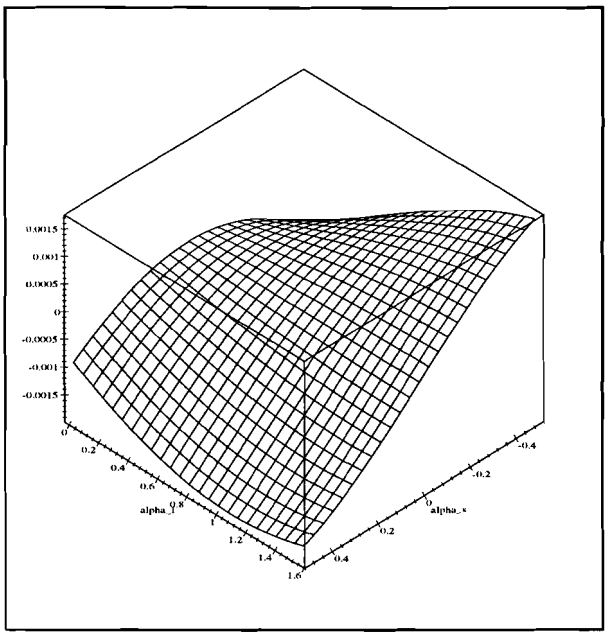

Figure 3.3: Deviation of the length (in mm.) the laser beam travels by a "side slip"

2. Wrong angle measurement

In Figure 3.2 is shown that the angle of the mirror will be changed, by a "side slip", to let the laser beam point again at the centre of the retro-reflector.

Computation of the deviation of the angle of the mirror by a "side slip" of the semi sphere

Angle of the deflected laser beam, without a "side slip":

$$\varphi = 2(\alpha_s + \alpha_l) - \frac{\pi}{2}$$

Angle of the deflected laser beam, by a "side slip":

$$\varphi' = \arctan\left(\frac{Yc - \delta'}{Xc}\right)$$

$$\varphi' = 2(\alpha_s + \alpha_l) - \frac{\pi}{2} - 2\Delta\alpha_s$$

Deviation of the angle of the mirror:

$$\Delta\alpha_s = \frac{1}{2}(\varphi - \varphi')$$

In Figure 3.4 the deviation of the angle (in rad.) of the mirror by a "side slip" is plotted, again with δ is 1 μm. Since it is known that the deviation is larger by a shorter measuring distance, the figure is plotted for the shortest measuring distance (r is 2 m). The deviation is also checked with a two times bigger δ. This result in a two times bigger deviation. From this may be concluded that the deviation is linear in δ.

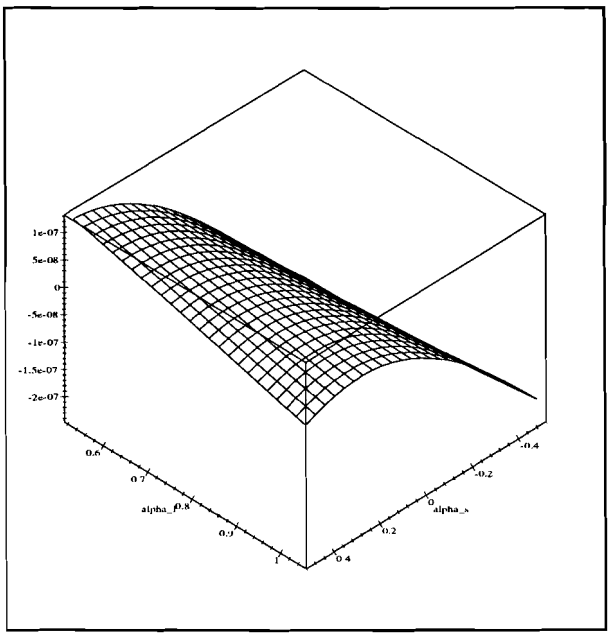

Figure 3.4: Deviation of the angle (in rad.) of the mirror by a "side slip" of the semi sphere

3.2 Effect of a variation of the air gap

The air gap (δ) of the semi sphere in its bearing seat is not constant during measuring. This means that the semi sphere moves in the direction perpendicular on the nominal position of the mirror surface, so also perpendicular on the movement of the "side slip", see Figure 3.5. For calculating this effect on the accuracy of the system, is assumed that the laser beam hits the centre of the retro-reflector.

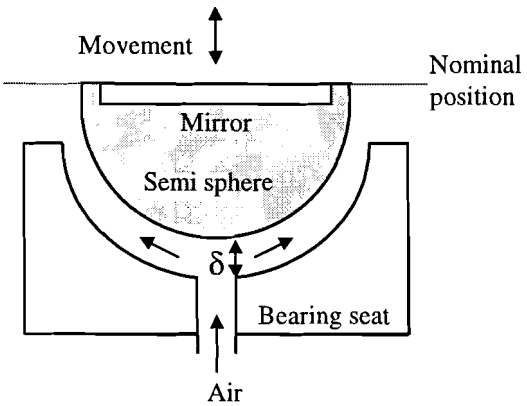

Figure 3.5: Top view of the semi sphere in its bearing seat

To give an impression of this effect, see Figure 3.6, where a two-dimensional schematic view is shown of an air gap variation.

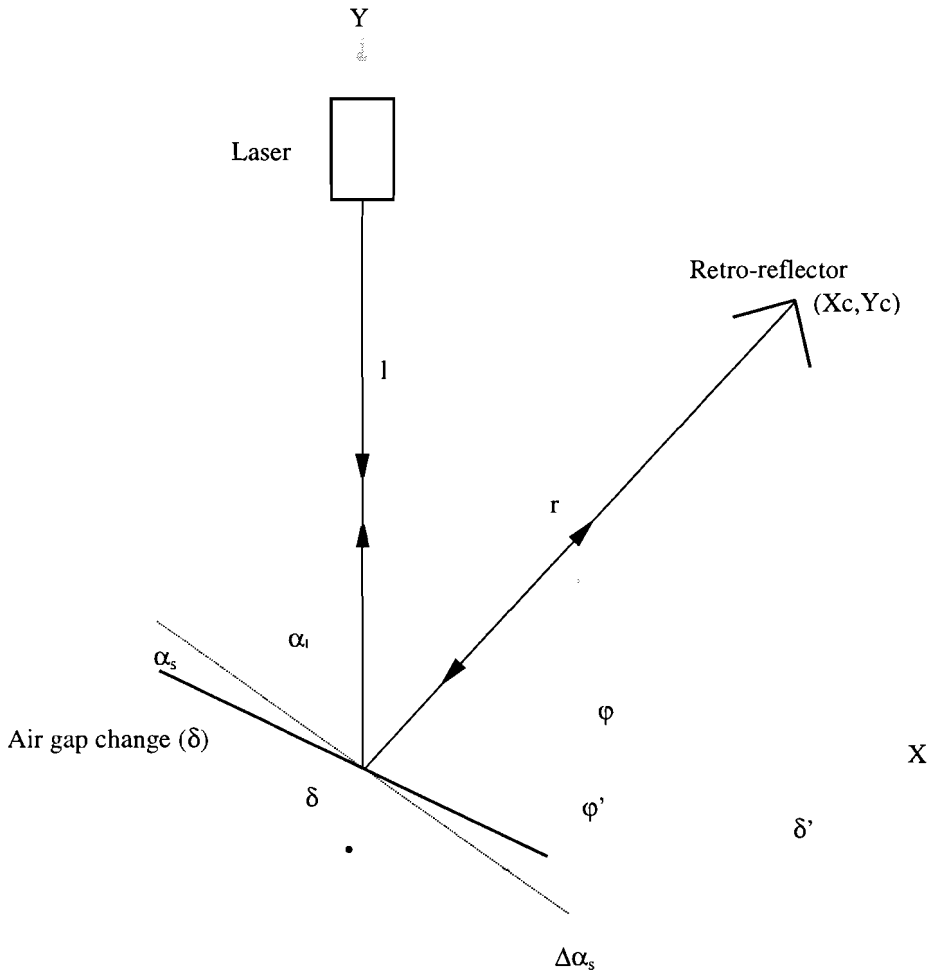

Figure 3.6: Variation of the air gap

Nominal position of the mirror

$\bullet \approx \alpha_l + \alpha_s$

Position of the mirror before air gap change

Position of the mirror after air gap change of distance δ, but before the corrected mirror-angle

Position of the mirror after air gap change and with corrected mirror-angle

When the air gap is not constant the accuracy of the system will be influenced in two ways:

1. ***Wrong distance measurement:*** *The distance the laser beam will travel during measuring is wrong by an air gap variation, because the laser beam travels another path.*
2. ***Wrong angle measurement:*** *When the air gap changes the laser beam will be deflected differently. So the angle of the mirror will be changed to let the laser beam point again at the centre of the retro-reflector.*

1. Wrong distance measurement

Computation of the deviation of the length the laser beam will travel by an air gap variation

Position retro-reflector: $Xc = r\cos\varphi$

$Yc = r\sin\varphi$

$$\varphi = 2(\alpha_s + \alpha_l) - \frac{\pi}{2}$$

Air gap variation: δ

Air gap variation in Y-direction:

$$\delta' = \frac{\delta \sin\left(\frac{\pi}{2} - \alpha_s\right)}{\sin(\alpha_s + \alpha_l)} \tag{3.3}$$

Travelled distance of the laser beam, by a constant air gap:

$$L_1 = 2(l + r)$$

Travelled distance of the laser beam, by an air gap variation:

$$L_2 = 2\{\ l + \delta' + \sqrt{Xc^2 + \{\ Yc + \delta'\ \}^2}\ \}$$

Deviation:

$$D = L_2 - L_1 = 2\{\ \delta' + \sqrt{Xc^2 + \{\ Yc + \delta'\ \}^2} - r\ \}$$

Deviation in first order approximation:

$$D \approx 2\delta'\{\ 1 + \sin\varphi\ \} \tag{3.4}$$

For this computation also holds that the deviation is independent from the measuring distance, if second and higher order terms be neglected.

In Figure 3.7 the deviation (in mm) of the length the laser beam travels by a variation of the air gap is plotted. The assuming value of δ is chosen 1 μm. From equation (3.3) and (3.4) may be concluded that the behaviour of the deviation is linear in δ.

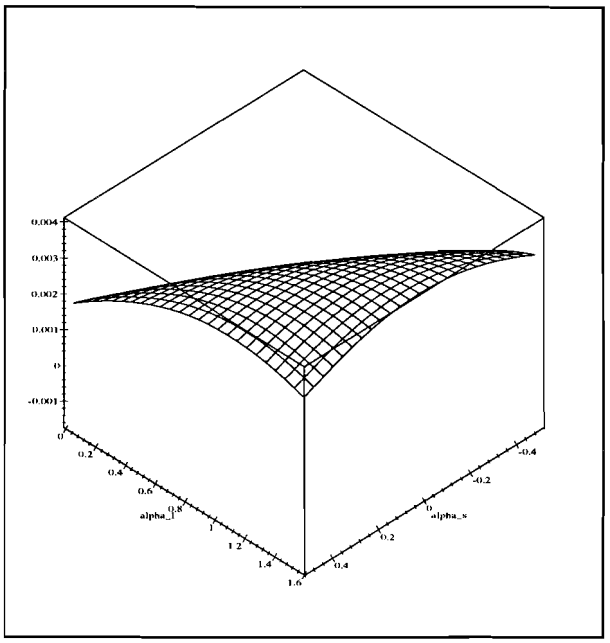

Figure 3.7: Deviation of the length (in mm.) the laser beam travels by an air gap variation

2. Wrong angle measurement

In Figure 3.6 is shown that the angle of the mirror will be changed, by an air gap variation, to let the laser beam point again at the centre of the retro-reflector.

Computation of the deviation of the angle of the mirror by an air gap variation

Angle of the laser beam to the retro-reflector, without an air gap variation:

$$\varphi = 2(\alpha_s + \alpha_l) - \frac{\pi}{2}$$

Angle of the deflected laser beam, by an air gap variation:

$$\varphi' = \arctan\left(\frac{Yc + \delta'}{Xc}\right)$$

$$\varphi' = 2(\alpha_s + \alpha_l) - \frac{\pi}{2} + 2\Delta\alpha_s$$

Deviation of the angle of the mirror: $\Delta\alpha_s = \frac{1}{2}(\varphi' - \varphi)$

In Figure 3.8 the deviation of the angle (in rad.) of the mirror by an air gap variation is plotted, again with δ is 1 μm and r is 2 m. The deviation is also checked with a two times bigger δ. This result in a two times bigger deviation. From this may be concluded that the deviation is linear in δ.

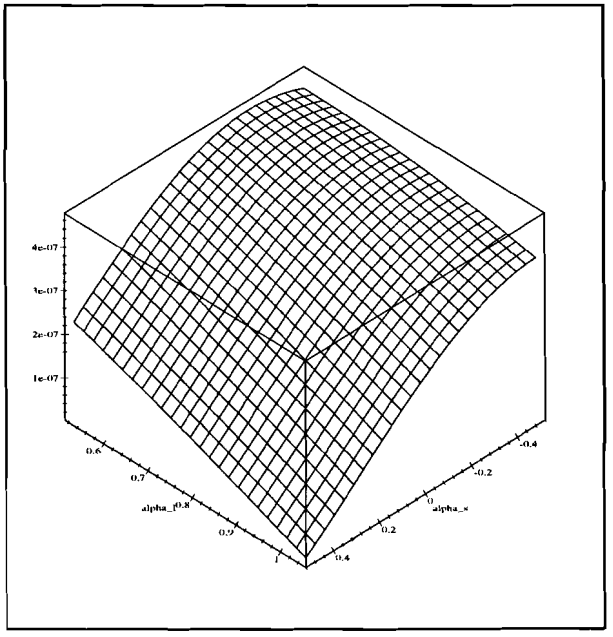

Figure 3.8: Deviation of the angle (in rad.) of the mirror by an air gap variation

3.3 Wrong alignment of the PSD

It is possible that the laser beam does not point exactly at the centre of the retro-reflector. This is the case for a wrong alignment of the PSD or errors in the calibrating phase, when an equilibrium centre is defined. Due to external influences, e.g. temperature variations, it is also possible that the laser beam will not point exactly at the centre of the retro-reflector. For calculating this effect on the accuracy is assumed that the deviation of the alignment of the PSD is δ. This means that the width between the incoming and deflected laser beam is also δ. Figure 3.9 gives a two-dimensional impression of this effect. For more details compared to the computation and the path the laser beam follows at the retro-reflector, see Appendix C: "The path of the laser beam at the retro-reflector when the alignment of the PSD is wrong."

When the alignment of the PSD is wrong the accuracy of the system will be influenced in two ways:

1. ***Wrong distance measurement:*** *The length the laser beam will travel differs from the length the laser beam travels when pointing at the centre of the retro-reflector, because the laser beam travels another path.*
2. ***Wrong angle measurement:*** *The laser beam does not point at the centre of the retro-reflector, so the measured angle of the mirror differs from the orientation of the retro-reflector.*

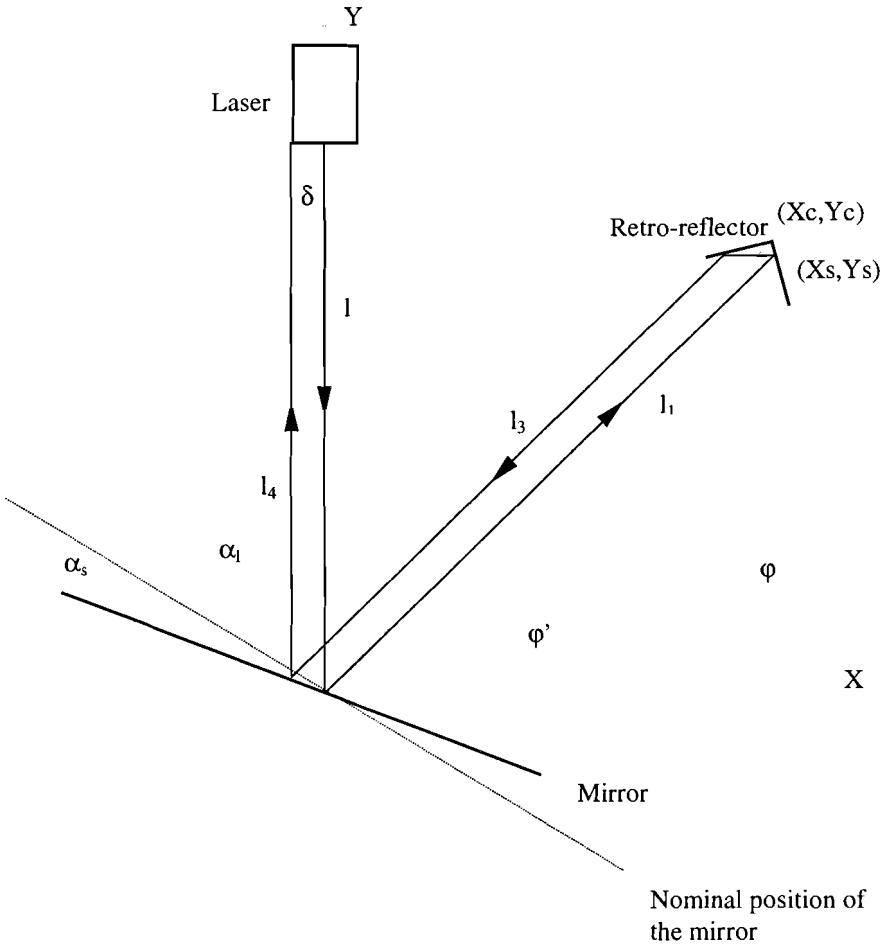

Figure 3.9: Wrong alignment of the PSD

1 Wrong distance measurement

Computation of the deviation of the length the laser beam will travel by a wrong alignment of the retro-reflector

Position retro-reflector:

$$Xc = r\cos\varphi$$
$$Yc = r\sin\varphi$$
$$\varphi = 2(\alpha_l + \alpha_s) - \frac{\pi}{2}$$

Incoming angle of laser beam at the retro-reflector:

$$\alpha_{ci} = \frac{\pi}{6} rad \ ^{1}$$

[1] Here is just filled in a value, because the deviation is independent of α_{ci}

Deviation of the alignment of the PSD: δ

Distance from the retro-reflectors centre: $d = \dfrac{\delta \sin\alpha_{ci}}{\sin 2\alpha_{ci}}$

Position of the incoming laser beam at the retro-reflector:

$$\phi = \varphi - \varphi' = \arcsin\left(\frac{d\sin\left(\frac{\pi}{2}+\alpha_{ci}\right)}{r}\right)$$

$$l_1 = \frac{r\sin\left(\frac{\pi}{2}-\alpha_{ci}-\phi\right)}{\sin\left(\frac{\pi}{2}+\alpha_{ci}\right)}$$

$$Xs = l_1\cos(\varphi-\phi)$$

$$Ys = l_1\sin(\varphi-\phi)$$

Rotation angle of the retro-reflector:

$$\alpha_c = \varphi' - \alpha_{ci}$$

Travelled distance of the laser beam, by pointing at the centre of the retro-reflector:

$$L_1 = 2(l+r)$$

Travelled distance of the laser beam, by not pointing at the centre of the retro-reflector:

$$L_2 = l + l_1 + l_2 + l_3 + l_4$$

With: $l_1 = \dfrac{r\sin\left(\frac{\pi}{2}-\alpha_{ci}-\phi\right)}{\sin\left(\frac{\pi}{2}+\alpha_{ci}\right)}$

$$l_2 = \frac{d}{\sin\alpha ci}$$

$$l_3 = \sqrt{\left(Xc - \sqrt{l_2^2 - d^2}\cos\alpha_c + \delta \right)^2 \left(1 + \tan^2(\varphi - \phi)\right)}$$

$$l_4 = \left(l - \delta \tan\left(\frac{\pi}{2} - \alpha_l - \alpha_s \right) \right)$$

Deviation:

$$D = L_2 - L_1$$

In Figure 3.10 the deviation (in mm) of the length the laser beam travels is plotted. Here is assumed that δ is 1 μm. The deviation is computed for a measuring distance of 2 m, because the deviation is larger for a smaller measuring distance. The deviation is also checked with a two times bigger δ. This result in a four times bigger deviation. From this may be concluded that the behaviour of the deviation is quadratic in δ.

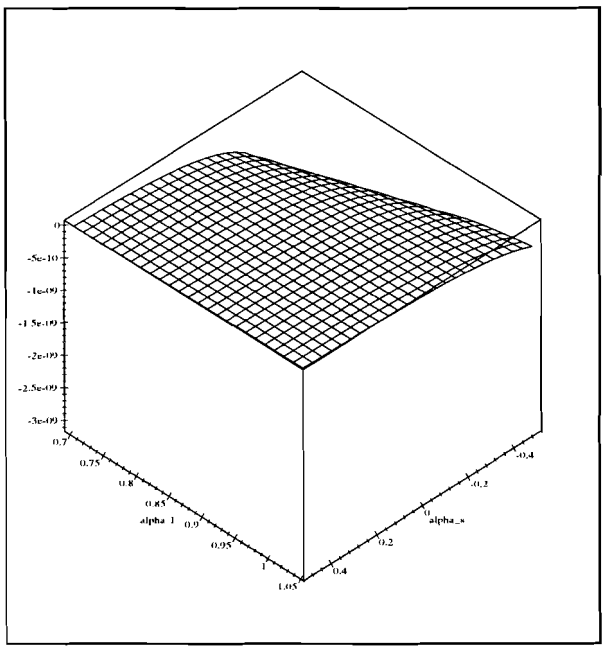

Figure 3.10: Deviation of the length (in mm.) the laser beam travels

2 Wrong angle measurement

Deviation of the orientation of the incoming laser beam at the retro-reflector:

$$\phi = \arcsin\left(\frac{d\sin\left(\frac{\pi}{2}+\alpha_{ci}\right)}{r}\right)$$

Deviation of the angle of the mirror:

$$\Delta\alpha_s = \frac{1}{2}\phi = \frac{1}{2}\arcsin\left(\frac{d\sin\left(\frac{\pi}{2}+\alpha_{ci}\right)}{r}\right) = \frac{1}{2}\arcsin\left(\frac{\delta\sin\alpha_{ci}\sin\left(\frac{\pi}{2}+\alpha_{ci}\right)}{r\sin 2\alpha_{ci}}\right) = \frac{1}{2}\arcsin\left(\frac{\delta}{2r}\right)$$

So the deviation of the angle of the mirror is larger for a smaller measuring distance (r). This means that the maximum value of $\Delta\alpha_s$ is reached for the smallest measuring distance.

For δ is 1 μm holds: $\Delta\alpha_{s(\max)} = \frac{1}{2}\arcsin\left(\frac{10^{-6}}{4}\right) = 0.125\cdot 10^{-6} rad$

3.4 The laser beam does not point at the centre of the mirror

For calculating this effect on the accuracy is assumed that the laser beam from the laser is pointed at the mirror with an angle error δ. This happens when the laser is not good aligned corresponding to the mirror or deviates due to external influences, such as temperature effects. Figure 3.11 gives a two-dimensional impression of this effect. Further is assumed that the laser beam hits the centre of the retro-reflector.

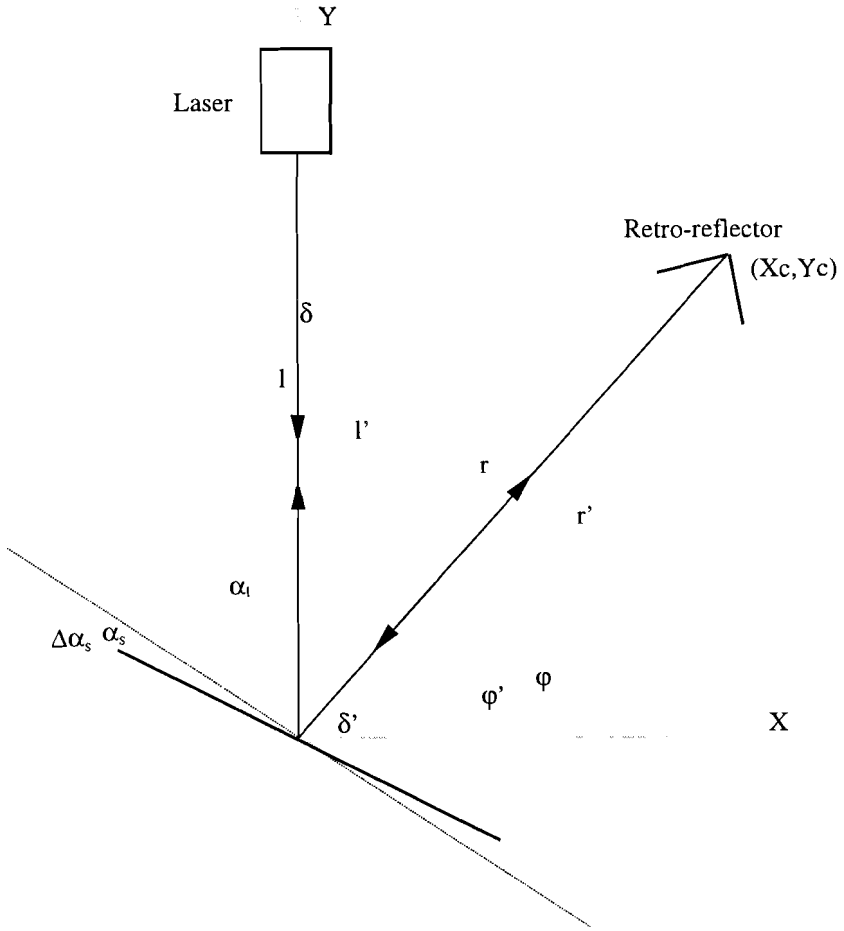

Fig. 3.11: The laser beam does not point at the centre of the mirror

Nominal position of the mirror

Position of the mirror, when the laser beam does point at the centre of the mirror

Position of the mirror, when the laser beam does not point at the centre of the mirror

The accuracy of the system is influenced in two ways:

1. ***Wrong distance measurement:*** *The distance the laser beam will travel during measuring is wrong, because the laser beam travels another path.*
2. ***Wrong angle measurement:*** *The angle of the mirror will be different when the laser does not point at the centre of the mirror, because the laser beam will be deflected different. To let the laser beam point again at the centre of the retro-reflector the angle of the mirror will be changed.*

1. Wrong distance measurement

Computation of the deviation of the length the laser beam will travel when the laser beam does not point at the center of the mirror

Position retro-reflector:

$$Xc = r\cos\varphi$$
$$Yc = r\sin\varphi$$
$$\varphi = 2(\alpha_s + \alpha_l) - \frac{\pi}{2}$$

Angle-error:

$$\delta = \arctan\left(\frac{\delta'}{l}\right)$$

Travelled distance of the laser beam from the laser to the mirror:

$$l' = \frac{l\sin(\pi - \alpha_l - \alpha_s)}{\sin(\alpha_l + \alpha_s - \delta)}$$

Travelled distance of the deflected laser beam from the mirror to the retro-reflector:

$$\Delta x = \delta' + \sin\delta\left(\frac{l\sin\delta\sin\left(\frac{\pi}{2} - \alpha_l - \alpha_s\right)}{\sin\left(\frac{\pi}{2} + \delta\right)\sin(\alpha_l + \alpha_s - \delta)}\right)$$

$$\Delta X = Xc - \Delta x$$

$$\Delta y = \cos\delta\left(\frac{l\sin\delta\sin\left(\frac{\pi}{2} - \alpha_l - \alpha_s\right)}{\sin(\alpha_l + \alpha_s - \delta)\sin\left(\frac{\pi}{2} + \delta\right)}\right)$$

$$\Delta Y = Yc + \Delta y$$

$$r' = \sqrt{(\Delta X^2 + \Delta Y^2)}$$

Travelled distance of the laser beam, by pointing at the centre of the mirror:

$$L_1 = 2(l + r)$$

Travelled distance of the laser beam, by not pointing at the centre of the mirror:

$$L_2 = 2(l' + r')$$

Deviation: $$D = L_2 - L_1$$

In Figure 3.12 the deviation (in mm) of the length the laser beam travels is plotted. The assuming value of δ' is chosen 1 mm. at a distance of 1 m. The deviation is computed for a measuring distance of 2 m., because the deviation is larger for a smaller measuring distance. The deviation is also checked with a two times bigger δ'. This result in a four times bigger deviation. From this may be concluded that the deviation is quadratic in δ'.

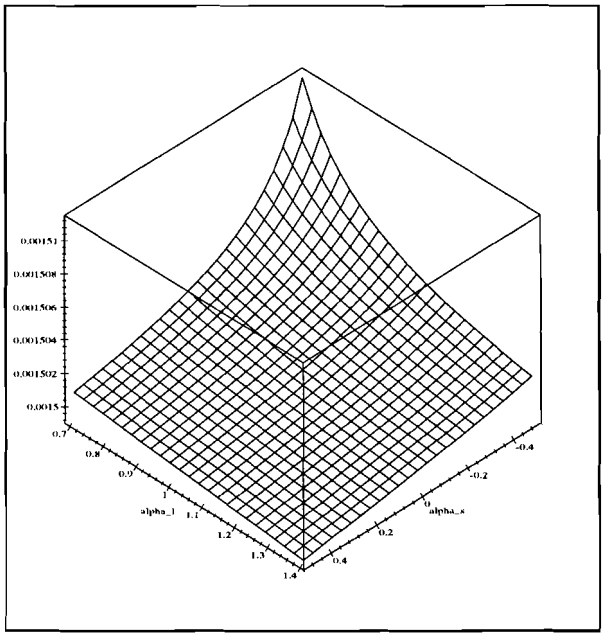

Figure 3.12: Deviation (in mm.) of the length the laser beam travels

2 Wrong angle measurement

Angle of deflected laser beam, by pointing at the centre of the mirror:

$$\varphi = 2(\alpha_s + \alpha_l) - \frac{\pi}{2}$$

Angle of deflected laser beam, by not pointing at the centre of the mirror:

$$\varphi' = \arctan\frac{\Delta Y}{\Delta X}$$

$$\varphi' = \varphi - \delta + 2\Delta\alpha_s$$

Deviation of the angle of the mirror:

$$\Delta\alpha_s = \frac{1}{2}(\varphi' + \delta - \varphi)$$

In Figure 3.13 the deviation of the angle (in rad.) of the mirror, when the laser beam does not point at the centre of the mirror is plotted, for δ' is 1 mm and r is 2 m. The deviation is also checked with a two times bigger δ'. This result in a two times bigger deviation. From this may be concluded that the behaviour of the deviation is linear in δ'.

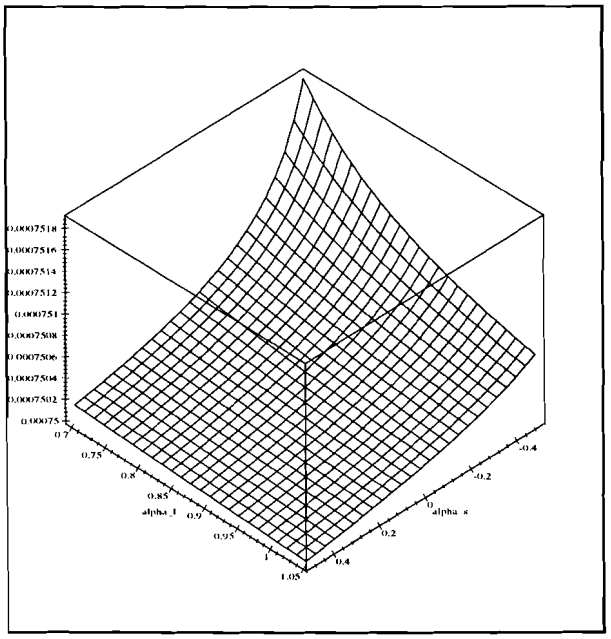

Figure 3.13: Deviation of the angle (in rad.) of the mirror

In Table 3.1 is given an overview of the several kinds of influences on the accuracy.

DEVIATION	INFLUENCE ON	VALUE OF THE DEVIATION	BEST VALUE FOR α_l (SMALLEST ERRORS)	EXPLAINING δ	BEHAVIOUR OF THE DEVIATION
A "side slip" of the semi sphere	Distance	Max. 2 δ	$0° < \alpha_l < 90°$	Side slip (in µm)	Linear
	Angle	$\Delta\alpha_s(max)$ = 0.12 µrad for δ=1µm	$30° < \alpha_l < 60°$		Linear
An air gap variation of the semi sphere in its bearing seat	Distance	Max. 4 δ	$1° < \alpha_l < 90°$	Air gap variation (in µm)	Linear
	Angle	$\Delta\alpha_s(max)$ = 0.46 µrad for δ = 1µm	$30° < \alpha_l < 60°$		Linear
Wrong alignment of the PSD	Distance	Max. 3.1 δ^2	$40° < \alpha_l < 60°$	Deviation of the alignment of the PSD (in µm)	Quadratic
	Angle	$\Delta\alpha_s(max)$ = 0.125 µrad for δ = 1µm	No influence		Linear
The laser beam does not point at the centre of the mirror	Distance	Max. 1.5 δ'^2	$40° < \alpha_l < 80°$	Angle error of the laser beam at the center of the mirror (in rad). δ' is the distance of the laser beam from the centre of the mirror (in mm) at a distance of 1 m.	Quadratic
	Angle	$\Delta\alpha_s(max) \cong$ 0.75 mrad for δ = 1 mrad	$40° < \alpha_l < 60°$		Linear

Table 3.1: Overview of computed deviations

From these computations may be concluded that:
- The deviations are small.
- $40° \leq \alpha_l \leq 60°$.

Subjoined follows some conclusions about the various computations.

- A "side slip" of the semi sphere

The "side slip" of the semi sphere is not controlled. A rough indication of the maximum "side slip" would be 1 µm.
This results in a maximum deviation for the distance measurement of: 2 δ = 2 µm.
And a maximum deviation for the angle measurement of: 0.12 · 1 = 0.12 µrad ≅ 1.2 µm, see also equation (3.5) on page 32.
The influence of the "side slip" on the deviation is acceptable.

- An air gap variation of the semi sphere in its bearing seat

To get an indication of the air gap variation of the semi sphere in its bearing seat due to tilting, we measured the air gap by tilting the mirror in different directions. We put a sine, with a frequency of 18 kHz, on one or both sides of the primary coil, see Figure 3.14. The effect on the air gap height can be obtained at output Hin.

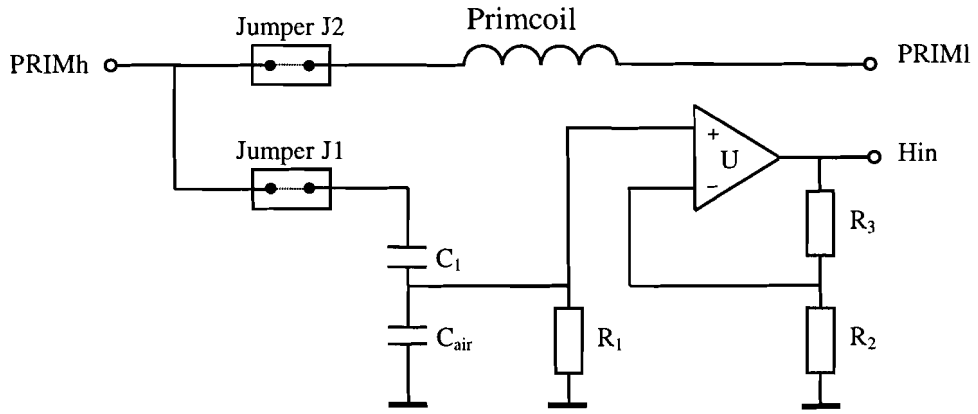

Figure 3.14: Air gap measurement variation

A maximum deviation of the air gap of 100 mV is measured. The sensitivity of the sensor is 11.4 nm/mV [LIN 98] for a gain of 11 at the mirror PCB. This means that the maximum variation of the air gap is 1.14 μm. The maximum deviation for the distance measurement is: $4\ \delta = 4.56$ μm. The maximum deviation for the angle measurement due to the air gap change is: $0.46 \cdot 1.14 = 0.5244$ μrad ≅ 5,244 μm.

The measurement of the angles of the mirror will also be influenced by a variation of the air gap. The movement induces a voltage over the secondary coils of the angle sensors. It is also possible that cross talk effects on the angle sensors and air gap sensor influences the measurement of the sensors.

- Wrong alignment of the PSD

For this computation holds that the influence on the measured distance may be neglected. The angle effect is significant. When the alignment of the PSD is not good, a rough indication of the deviation would be 1 mm. This results in a maximum angle error of 125 μrad. We may conclude that the error is too big, so the alignment or calibration of the PSD should be done. An acceptable deviation of the alignment would be 20 μm, which results in a deviation of an angle measurement of 2.5 μrad ≅ 25 μm.

- The laser beam does not point at the centre of the mirror

For this computation also holds that the influence on the distance may be neglected. Without aligning the laser to the mirror it is possible that the deviation is about 1 mm at a distance of 1 m. This deviation results in an unacceptable maximum angle error of 750 μrad.
The conclusion is that the system should be aligned to take care that the laser beam points at the centre of the retro-reflector with a maximum acceptable deviation of 5 μm. This results in a deviation of angle measurement of 3.75 μrad ≅ 37.5 μm.

3.5 Inaccuracies of the optical components

The optical components used for the laser tracking system are:
- Laser.
- Laser interferometer.
- Retro-reflector.
- Beam-splitter.
- PSD.

- Laser

For an interferometer it is important that the frequency and the phase of the light source stays at a constant value, because this is the cause of an inaccuracy. For lasers holds that the deviation of the frequency is very small contrary to other light sources.

- Laser interferometer

The following information about the accuracy of laser interferometry is known from [SCH 86].
The accuracy of laser interferometry depends on:
* The accuracy of the counting of the interference's
* The accuracy of the refractive index of air
* The stability of the frequency of the laser and the value of the frequency

In formula this means:
$$\frac{d\Delta l}{\Delta l} = \frac{d(p+a)}{p+a} - \frac{dn}{n} - \frac{df}{f}$$

{ $\Delta l = (p+a)\frac{\lambda}{2}$ with $0 \le a \le 1$, $\lambda \approx 0.6$ µm, p = # pulses, Δl = measured distance }

For a laser holds that:
$$\frac{df}{f} = -\frac{d\lambda}{\lambda} \le 10^{-8}$$

The refractive index of air depends on the temperature, air pressure and the composition of the air.
According to Edlén it is possible with his relations to compute the refractive index of air, by neglecting the influence of temperature and air composition, with the following inaccuracy:
$$\frac{dn}{n} \le 5 \cdot 10^{-8}$$

For large measuring distances (Δl) holds that $p+a \approx p$.

Then holds that:
$$\frac{d(p+a)}{p+a} \le \frac{dp}{p} \le \left(\frac{dp}{p}\right)_{max} \le \frac{1}{p} \le 10^{-7}$$

The total accuracy of a laser interferometer is: $\frac{d\Delta l}{\Delta l} \le 10^{-6}$

- Retro-reflector

According to the R&D department of LEICA, the producer of the retro-reflector, the beam deviation from the incoming and deflected laser beam is 5-10″ (= δ = *), see Figure 3.15. This is about 48.5 μrad.

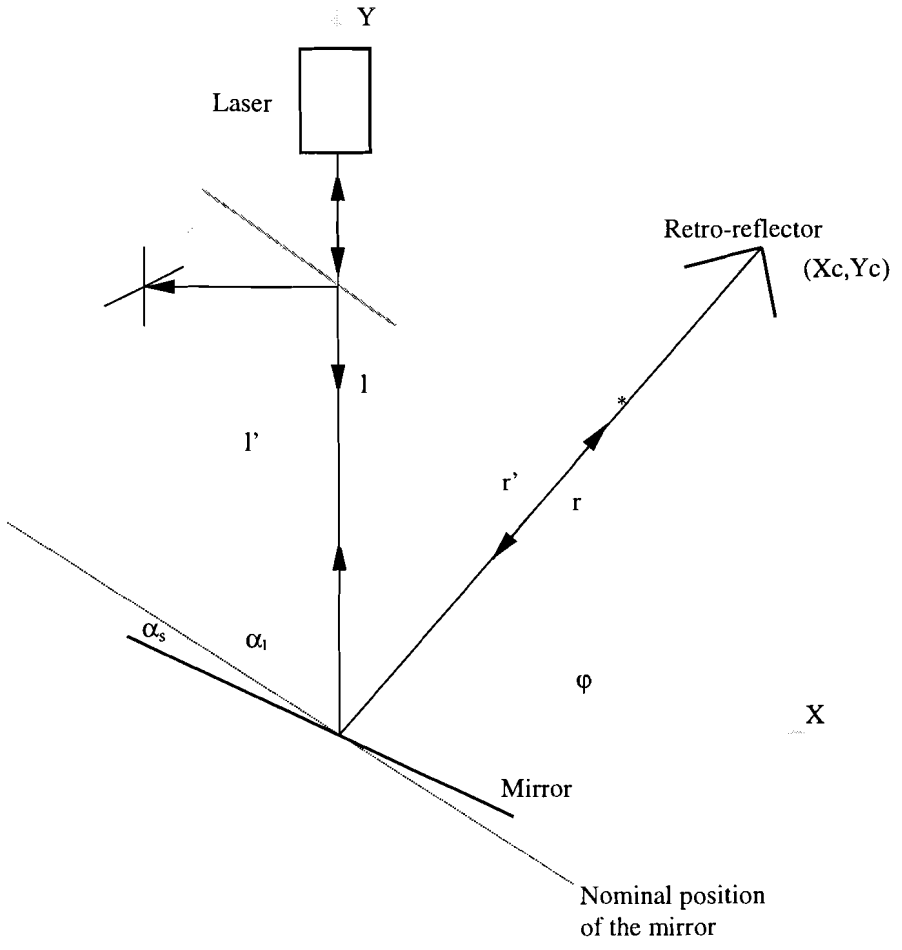

Figure 3.15: The influence of a beam deviation of the retro-reflector

What this means for the travelled distance of the laser beam is calculated in the following computation.

Position retro-reflector:

$$Xc = r\cos\varphi$$
$$Yc = r\sin\varphi$$
$$\varphi = 2(\alpha_s + \alpha_l) - \frac{\pi}{2}$$

Beam deviation: $\delta_{max} = 10'' \cong 48.5 \cdot 10^{-6}$ rad.

Travelled distance of the laser beam for an ideal retro-reflector (δ = 0):

$$L_1 = 2(l + r)$$

Travelled distance of the laser beam for a retro-reflector with a beam deviation of 48.5 μrad.:

$$L_2 = l + r + r' + l'$$

With: $$r' = \frac{r\sin(\pi - \alpha_l - \alpha_s)}{\sin(\alpha_l + \alpha_s - \delta_{max})}$$

$$l' = \frac{l - x\cos(\alpha_l + \alpha_s)}{\cos\delta_{max}} \text{ and } x = \frac{r\sin\delta_{max}}{\sin(\alpha_l + \alpha_s - \delta_{max})}$$

Deviation: $$D = L_2 - L_1$$

In Figure 3.16 the deviation in (mm) of the length the laser beam travels is plotted. The deviation is computed for a measuring distance of 10 m, because the deviation is larger for a larger measuring distance.

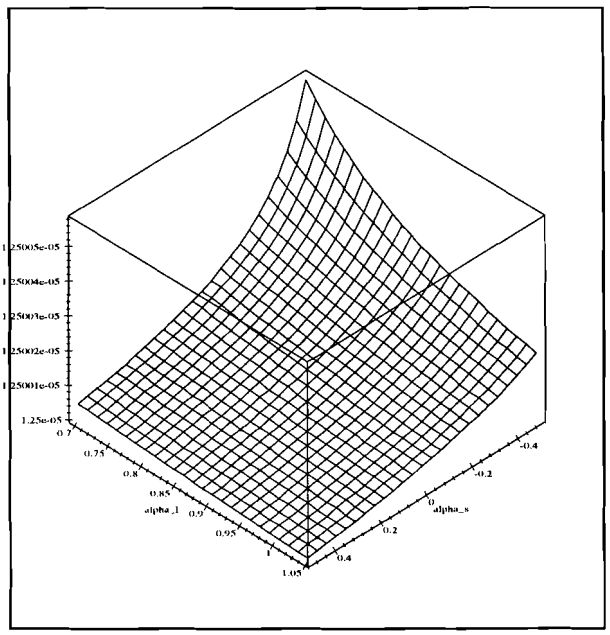

Figure 3.16: Deviation (in mm.) of the length the laser beam travels

We may conclude that the deviation of the length the laser beam travels as a result of a beam deviation of the retro-reflector can be neglected.

- Beam-splitter

Because of the beam-splitter the intensity of the laser beam decreases with 50% every time the laser beam passes the beam-splitter. This means that the intensity of the laser beam on the PSD is only 25% of the original intensity of the original beam. Here is expected that the absorption coefficient of the beam-splitter is zero. Because of a few percent absorption in practice, the light intensity of the laser beam on the PSD would be a few percent less than 25%.

- PSD

It is already known that an optical filter is needed in front of the PSD, because the daylight and the TL-light cause a lot of noise [LIN 98].
The output current/Watt light of the PSD is sensitive enough for a wavelength of a He-Ne-laser (≈633 nm), see Figure 3.17. The light intensity of the laser beam that is projected at the PSD is bounded to a maximum of 94 mW. The PSD may receive a maximum of 30000 W/m^2. The spot has a radius of approximately 1 mm.
Therefore the light intensity is bounded to a maximum of $\pi \cdot (1 \cdot 10^{-3})^2 \cdot 30000 \approx 94$ mW. The current laser used has a light intensity of 0.5 mW.

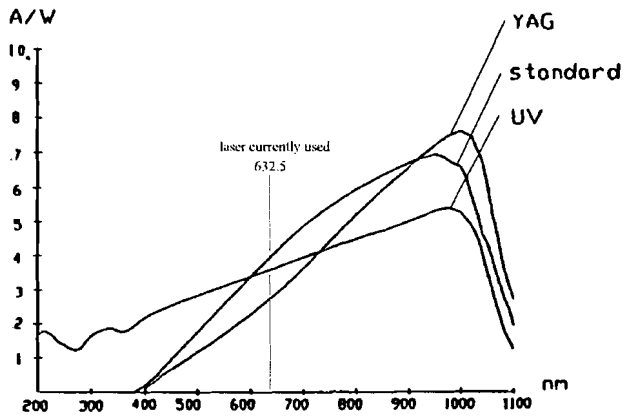

Figure 3.17: Output current/watt light as function of the wavelength

With the set-up of the laser tracking system it is already explained that the received power of the laser beam by the PSD is only a quarter of the emitted power. The light intensity of the laser has to be taken such that the maximum allowable intensity is received by the PSD to maximise the signal to noise ratio.
Table 3.2 shows the light sensor parameters of the PSD.

The bottleneck of the inaccuracy is caused by the used electronic. Currently the OT-300DL amplifier is used. More information can be read in [LIN 98].

Parameter	Light sensor (SiTek 2L10SP)
Non-linearity	±0.3%
Thermal drift	20-40 ppm/°C
Resolution	0.1 ppm
Rise time	0.2 µs
Spectral response	Figure 3.17 (standard)

Table 3.2: The light sensor parameters of the PSD

3.6 Inaccuracies caused by external influences

The temperature causes the most important external influence on the accuracy. From measurements from [LIN 98] may be concluded that it is necessary that the optical components of the laser tracking system have to be in a box with a constant temperature. The measured temperature drift for the sensors are ≈ 1 mV/hour according to [LIN 98].
The mechanical parts of the system have a coefficient of linear thermal expansion of k · 10^{-5} m/°C (k depends on the kind of material and is about 1...3).

3.7 Sensitivity of the sensors

- Angle sensors

A rough indication of the sensitivity is 43.6 µrad/mV [LIN 98]. A resolution of 5 mV would be equal to 218 µrad. The opening angle of the mirror is 5/18 · π rad ($-25° \leq \alpha_s \leq 25°$). At a distance of 10 m this results in an arc-length of 50/18 · π m.

This means that: $$\frac{5}{18}\pi[rad] \cong \frac{50}{18}\pi[m] \tag{3.5}$$

$$1[rad] \cong 10[m]$$

$$218[\mu rad] \cong 2.18[mm]$$

With the angle sensors it is possible to measure with a sensitivity of 2.18 mm at a distance of 10 m. This sensitivity is enough for the scanning mode.

- Air gap sensor

The sensitivity of the air gap sensor is 11.4 nm/mV [LIN 98]. The noise is about 5 mV, so the sensor's resolution is 57 nm. We may conclude that the sensor's resolution is enough for measuring the air gap.

3.8 The influence of a position displacement of the retro-reflector on the PSD

Besides all the computations for the accuracy analysis it is also important to know the maximum displacement of the retro-reflector with a stationary mirror for which holds that the laser beam still can be detected by the PSD, see also Figure 3.18.

Position of the retro-reflector:

$$Xc = r\cos\varphi$$
$$Yc = r\sin\varphi$$
$$\varphi = 2(\alpha_s + \alpha_l) - \frac{\pi}{2}$$

Incoming angle of laser beam:

$$\alpha_l = \frac{\pi}{4} rad^2$$

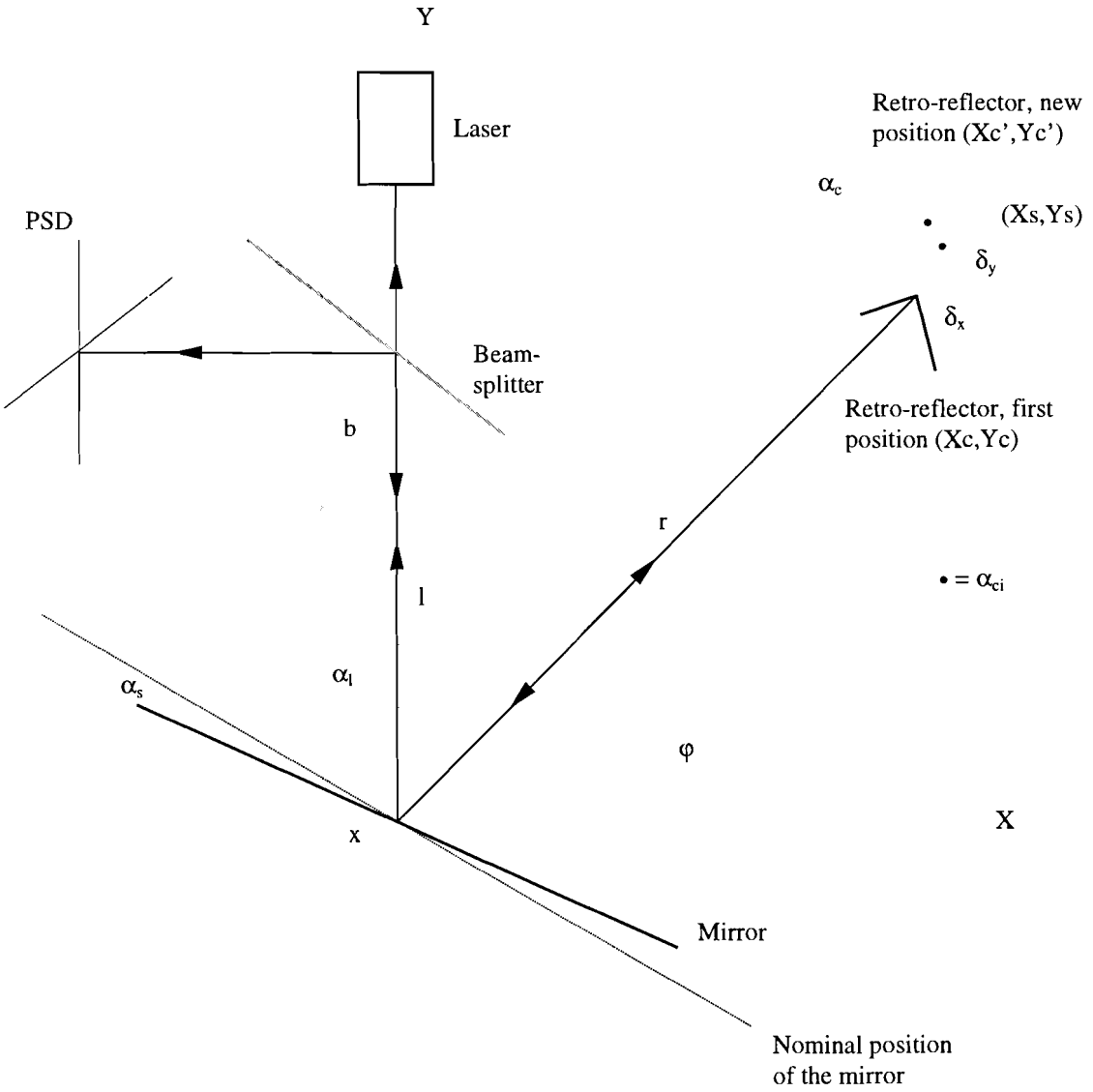

Figure 3.18: The influence of a position displacement of the retro-reflector

[2] Here is just filled in a value because the graphs only shifts along the axis, but the maximum value stays the same.

Displacement of the retro-reflector in X-direction: δ_x

Displacement of the retro-reflector in Y-direction: δ_y

Displacement of the retro-reflector: $\delta = \sqrt{\delta_x^2 + \delta_y^2}$

Position of the retro-reflector after displacement:

$$Xc' = Xc + \delta_x$$

$$Yc' = Yc + \delta_y$$

Position of the laser beam on the retro-reflector:

$$\left(\tan\alpha_c = \frac{Xs - Xc'}{Yc' - Xs\tan\varphi} \right)$$

$$Xs = \frac{Xc' + Yc'\tan\alpha_c}{1 + \tan\varphi\tan\alpha_c}$$

$$Ys = Xs\tan\varphi$$

Angle of the retro-reflector: $\alpha_c = \varphi - \alpha_{ci}$

Distance from retro-reflector's centre:

$$d = \sqrt{(Xs - Xc')^2 + (Ys - Yc')^2}$$

In Figure 3.19 the distance from the retro-reflector's centre is plotted for $\delta_x = \delta_y = 0.5$ mm.

Distance between incoming and reflected laser beam at the retro-reflector:

$$b = \frac{d\sin 2\alpha_{ci}}{\sin\alpha_{ci}}$$

In Figure 3.20 the width between incoming and reflected laser beam is plotted for $\delta_x = \delta_y = 0.5$ mm.

Distance of the laser beam from the mirror's centre:

$$x = \frac{b}{\sin(\alpha_l + \alpha_s)}$$

Figure 3.21 shows the deviation of the laser beam from the centre of the mirror for $\delta_x = \delta_y = 0.5$ mm.

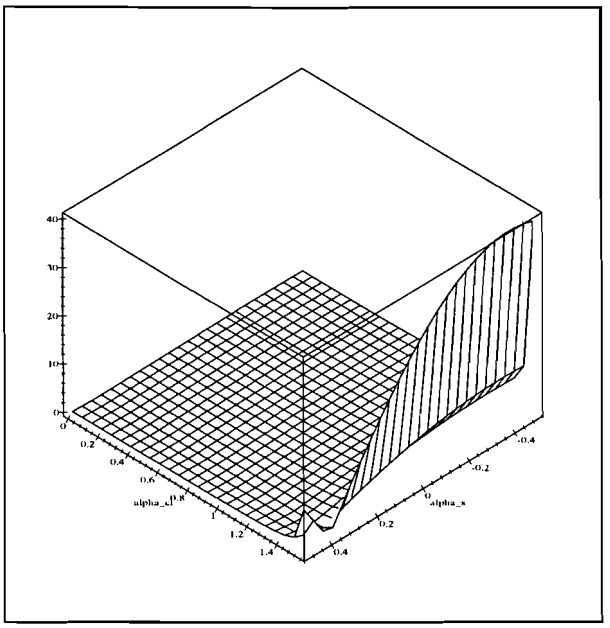

Figure 3.19: Distance (in mm.) of the laser beam from retro-reflector's centre

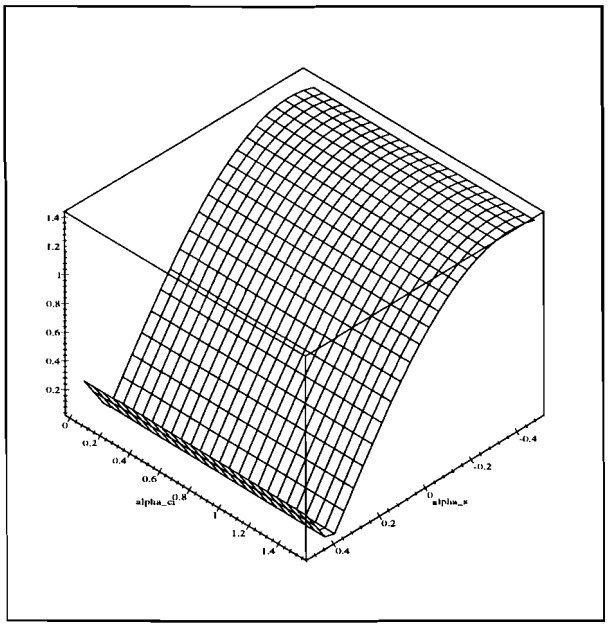

Figure 3.20: Distance (in mm.) between incoming and reflected laser beam

For this displacements holds that b has its maximum value for α_s is -25°.

We can conclude that generally holds that:

$$b_{\max} = 2\sqrt{\delta_x^{\,2} + \delta_y^{\,2}}$$

The maximum value of d is reached for large values of α_{ci}.

$$d_{\max} = \frac{b \sin \alpha_{ci}}{\sin 2\alpha_{ci}}$$

$$d_{\max}\left(\alpha_{ci \to 90°}\right) = \infty$$

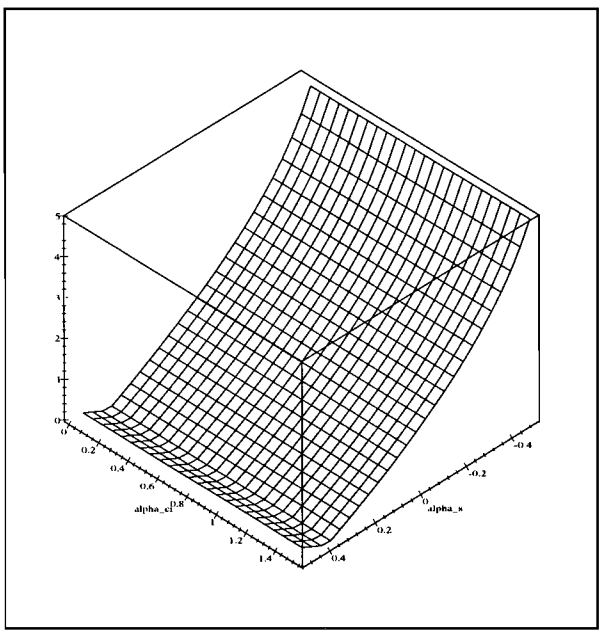

Figure 3.21: Distance (in mm.) from mirror's centre

The maximum range of the mirror is reached before the laser beam reaches the maximum active area of the PSD. The maximum displacement of the retro-reflector for the mirror with a radius of 5 mm would be:

$$\sqrt{\delta_x^{\,2} + \delta_y^{\,2}} = \sqrt{\left(\frac{1}{2}\right)^2 + \left(\frac{1}{2}\right)^2} = \frac{1}{2}\sqrt{2}mm \approx 0.7mm$$

The maximum deviation of the laser beam from the PSD's centre is in this case:

$$2\sqrt{\delta_x^{\,2}+\delta_y^{\,2}} = 2\sqrt{\left(\frac{1}{2}\right)^2+\left(\frac{1}{2}\right)^2} = \sqrt{2}mm \approx 1.40mm$$

The deviation of the laser beam from the centre of the retro-reflector is in this case acceptable when $\alpha_{ci} \leq 85°$.

$$d = \frac{b\sin\alpha_{ci}}{\sin 2\alpha_{ci}} = \frac{\sqrt{2}\sin 85°}{\sin 170°} \approx 8.11mm$$

4. H_∞ Air gap controller

To guarantee the accuracy of the laser tracking system, it is important to keep the air gap of the semi sphere in its bearing seat on a constant value for a bandwidth wider than the disturbing effects of mirror rotations. There is chosen for an H_∞ controller because, with this controller it is possible to define and quantify the control aims very clearly by weighting them relatively.

4.1 Measurement of the transfer function of the process

The block scheme of the system that controls the air gap of the semi sphere in its bearing seat is shown in Figure 4.1. With the voltage V_0 and the air pressure a starting value for the air gap (g_0) can be realised. HcR is the input signal for the actuators and Hm corresponds with the measured air gap variation (g).

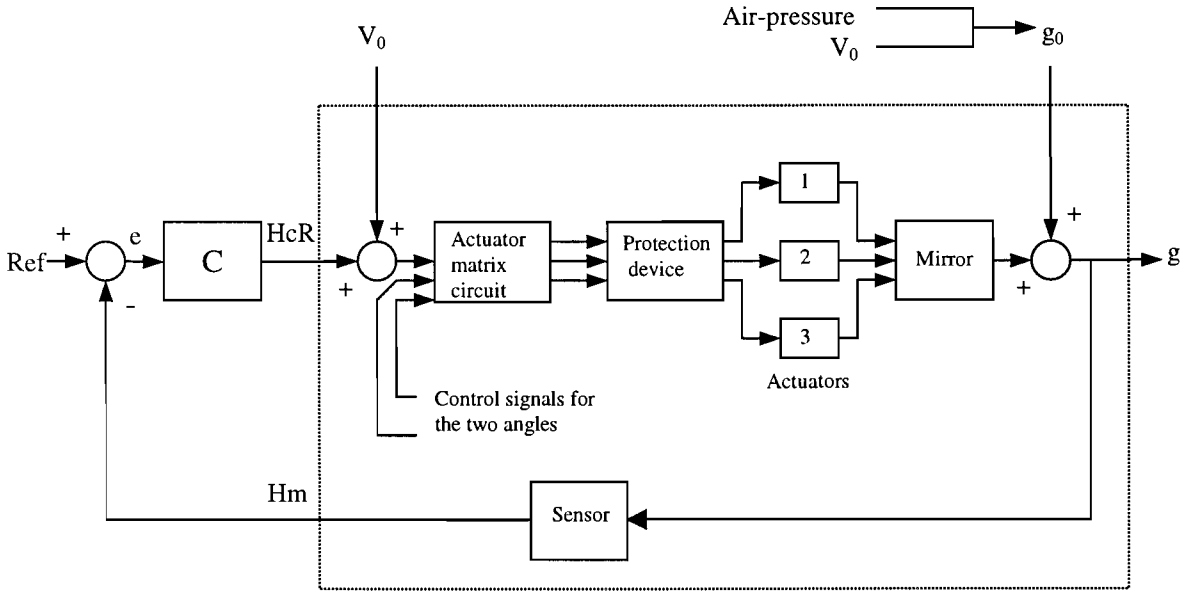

Figure 4.1: Block scheme of air gap control system

The actuator matrix circuit computes the voltages for the three actuators, such that the air gap height and the horizontal and vertical deflection of the mirror can be realised. The protection device protects the system against too high voltages.

The process P(s) is now defined as: $$P(s) = \frac{Hm(s)}{HcR(s)}$$

With a spectrum analyser the frequency response of P(s) was measured, see [LIN 98]. With Testlab the data from the spectrum analyser were transferred to the PC and the measurements were combined to one file and used to calculate the transfer function. The result is shown in Figure 4.2. Figure 4.3 gives the pool zero map of the process.

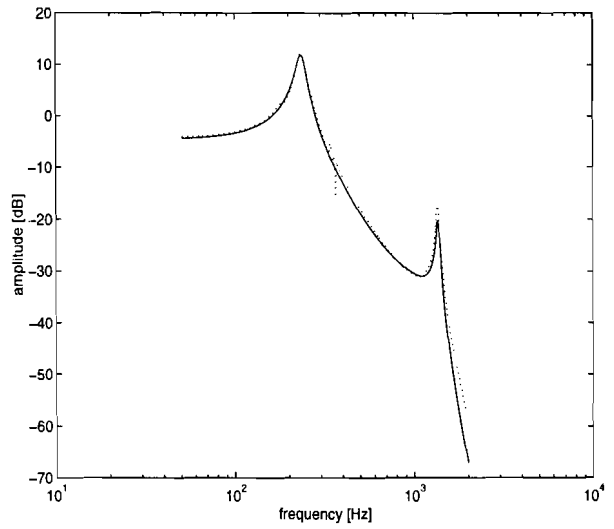

Figure 4.2: Measured transfer function of identified process.

The dotted line corresponds with the real measured data and the solid line is the fitted data by MATLAB.

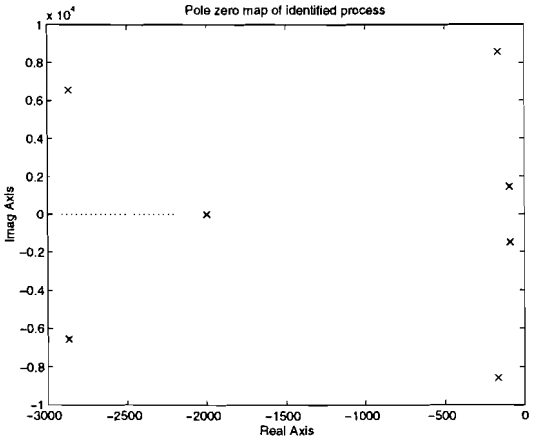

Figure 4.3: Pole-zero map of identified process.

These measurements hold for a particular value of the air gap g (g_0 = 27.8 μm). This set point was defined by the tension of the pretension springs. The resonance frequencies at about 350 Hz are not modelled. The controller should attenuate these resonance frequencies. From measurements we can conclude that these resonance frequencies are caused by the actuators, because these are not influenced by an air gap variation. It would be very hard to model the resonance frequencies. Besides that is it more important to move the resonance frequency at about 210 Hz to a higher frequency, by increasing the spring constant of the pretension springs. This resonance frequency depends namely on the mass of the actuator and the spring constant of the pretension springs. The resonance frequency at about 1500 Hz is a combination of the mass of the mirror, the tension of the twaron strings and the spring constant which models the air gap effects.

Two controllers are designed:

1. A controller designed with a reduced 3rd order model of the process. In this case the 3 most relevant poles of the process are taken.

2. A controller designed for the 7th order model of the process.

4.2 Block scheme with shaping and weighting filters

In Figure 4.4 a general controlling block scheme is extended with shaping and weighting filters.

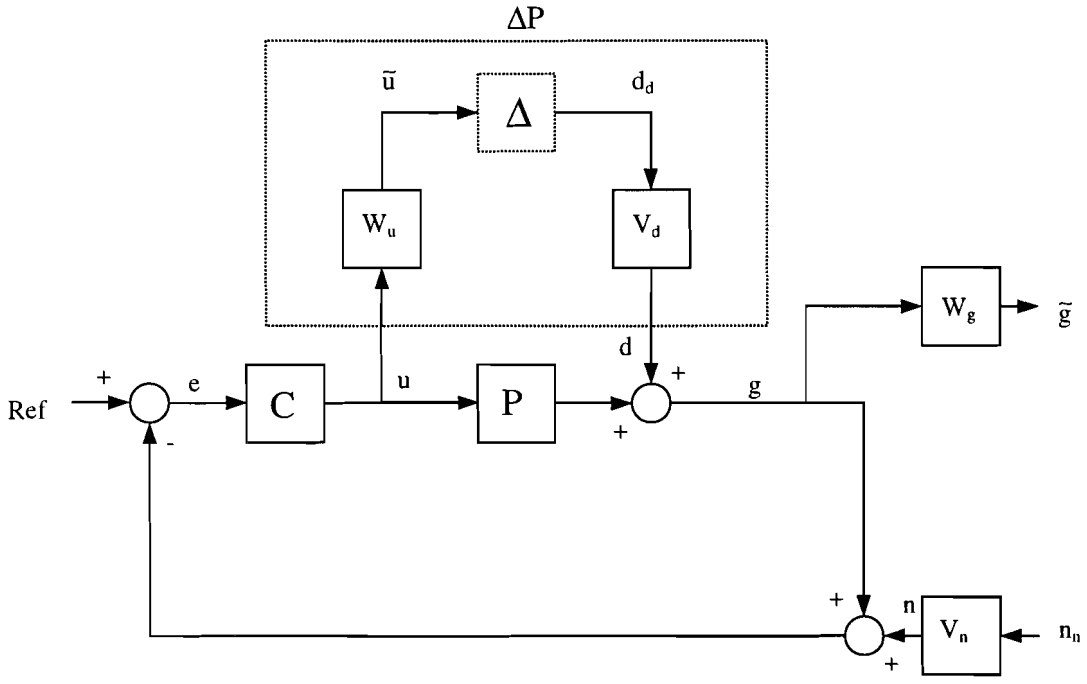

Figure 4.4: Block scheme with shaping and weighting filters

The block ΔP represents the additive model perturbations of the process with $\|\Delta\|_\infty < 1$.

ΔP is determined by:

Limited identification:	The measurement of the transfer function of the process can not be done without an error.
Unmodelled dynamics:	The process is approximated by a simple representation. The resonance frequencies caused by the actuators, of Figure 4.2 at about 350 Hz are not modelled.
Time variance:	The dynamics of the process change in time due to the influence of change in air pressure or temperature.
Model reduction:	In case of a third order approximation of the process.

Figure 4.5 gives the model perturbation of the reduced 3rd order model . ΔP is defined as an error made during the fitting of the measured data and an error made cause of the approximation of the process by a third order model.

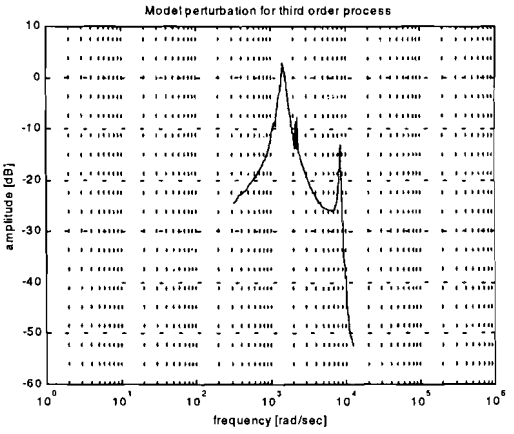

Figure 4.5: Model perturbation 3rd order model of the process

Figure 4.6 gives the model perturbation of the 7th order model . ΔP is in this case defined as the error made during fitting of the data.

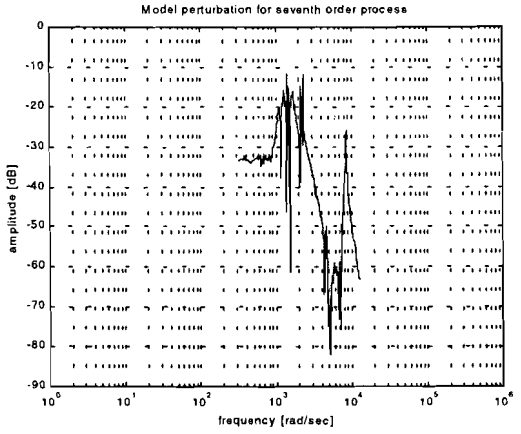

Figure 4.6: Model perturbation 7th order model of the process

To meet desired performance objectives in H_∞ control system design it is possible to augment the process by choosing appropriate weights on the signals entering and leaving the control configuration. These weightings of inputs and outputs results in respectively shaping and weighting filters.

The shaping filters

- V_n

This filter represents the sensor noise.

• V_d
Shaping filter V_d characterises the disturbance on the air gap height. The disturbance consists of disturbances due to the mentioned model perturbation |ΔP| and the disturbances of the air gap height, when the mirror is rotated. The last mentioned disturbance (100 mV) has been measured and written down in section 3.4 on page 27.

The weighting filters

• W_u
Weighting filter W_u weights the actuator signal u. This filter represents the model perturbation and should protect the actuator against saturation.

• W_g
Weighting filter W_g weights the deviation of the actual air gap of the process.

4.3 The augmented plant

The block scheme of Figure 4.4 results in the following augmented plant:

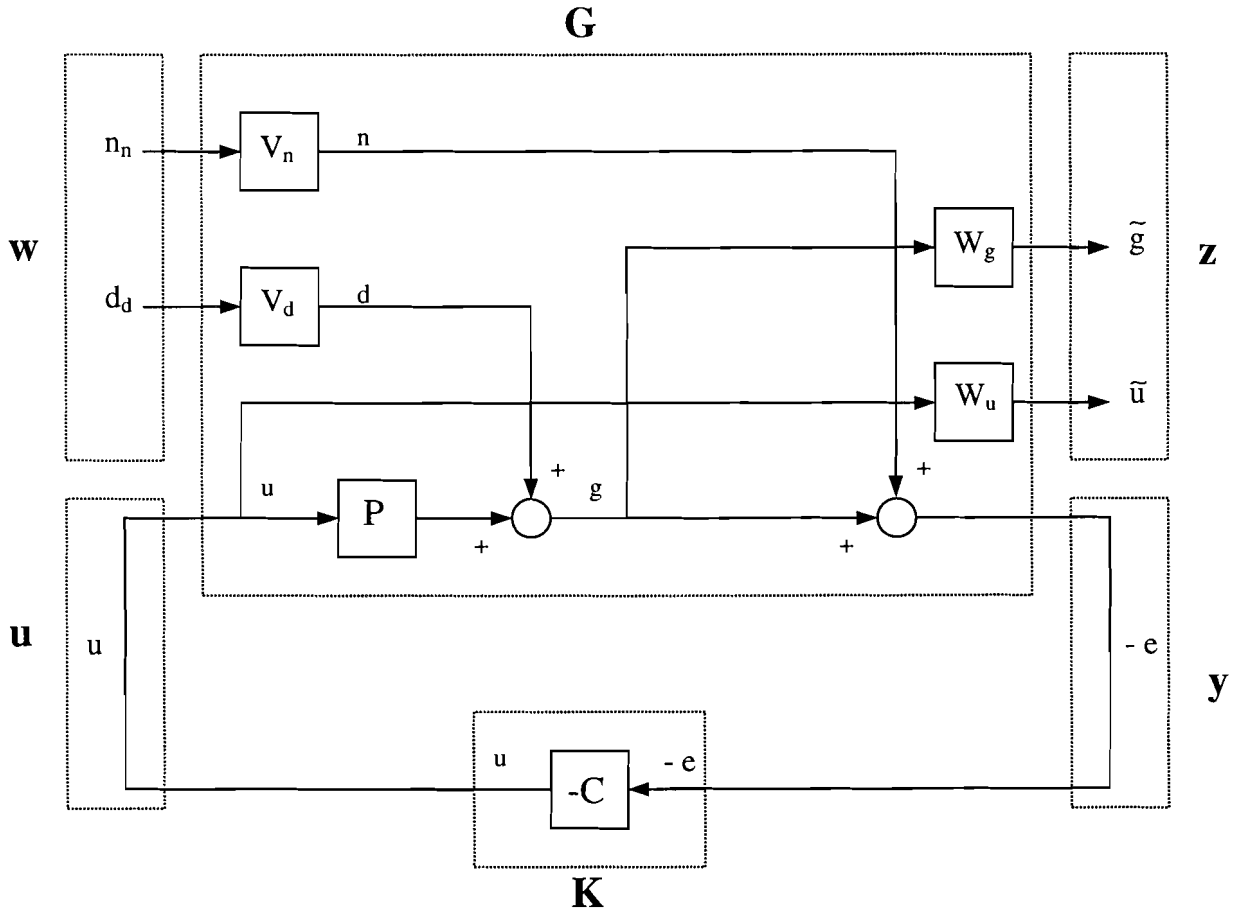

Figure 4.7: The augmented plant of the air gap control system

In the augmented plant **w**,**z**,**y** and **u** are vectors. The exogenous inputs are collected in **w** and are $£_2$ - bounded signals. These signals are shaped by V - filters before entering the system. The output signals are collected in **z**. These signals have to be minimised in $£_2$ - norm, after weighting by the W - filters. The measured output **y** is used as input signal of the controller to be designed. The controller generates the output **u**.
This signal is applied to the augmented system with transfer function G(s). In s - domain we may write the augmented plant in the following form:

$$\begin{pmatrix} z \\ y \end{pmatrix} = \begin{pmatrix} G_{11} & G_{12} \\ G_{21} & G_{22} \end{pmatrix} \cdot \begin{pmatrix} w \\ u \end{pmatrix}$$

While the controller is denoted by: $u = K \cdot y$

Eliminating **u** and **y** yields:

$$z = \left[G_{11} + G_{12}K(I - G_{22}K)^{-1}G_{21}\right]w = M(K)w$$

The control aims requires:

$$\min_{K\text{stabilising}} \sup_{w \in £_2} \frac{\|z\|_2}{\|w\|_2} = \min_{K\text{stabilising}} \|M(K)\|_\infty \tag{4.1}$$

Where: $$\|s\|_2 = \sqrt{\int_0^\infty |s(t)|^2 dt}$$

is the two norm, which expresses the energy of the signal s(t).

The interpretation of the left side of equation (4.1) is as follows:
Above all, there has to be found a stabilising controller K. In this equation "sup w $\in$ $£_2$" indicates that w is a worst disturbance, which is however bounded. For this worst disturbance, the energy of z, containing the air gap g and the actuator signal u, should be minimised.

If we have several transfers properly weighted, they can be taken as entries m_{ij} in the matrix M like:

$$M = \begin{pmatrix} m_{11} & m_{12} & \cdots \\ m_{21} & \ddots & \vdots \\ \vdots & \cdots & \ddots \end{pmatrix}$$

and then it holds that: $$\|m_{ij}\|_\infty \le \|M\|_\infty$$

Consequently the condition: $$\|M\|_\infty < 1$$

is sufficient to guarantee that: $$\forall i,j : \|m_{ij}\|_\infty < 1$$

So the $\|\cdot\|_\infty$ of the full matrix M bounds the $\|\cdot\|_\infty$ of the various entries.

From the augmented plant we can determine the following closed loop transfer matrix M:

$$M = \begin{pmatrix} \frac{\tilde{g}}{n_n} & \frac{\tilde{g}}{d_d} \\ \frac{\tilde{u}}{n_n} & \frac{\tilde{u}}{d_d} \end{pmatrix} = \begin{pmatrix} W_g \cdot \frac{PK}{I-PK} \cdot V_n & W_g \cdot \frac{I}{I-PK} \cdot V_d \\ W_u \cdot \frac{K}{I-PK} \cdot V_n & W_u \cdot \frac{K}{I-PK} \cdot V_d \end{pmatrix} \tag{4.2}$$

When it is realised to obtain:

$$\|M\|_\infty < \gamma \approx 1$$

Then it can be guaranteed that:

$$\forall \omega \in \Re: \quad \begin{pmatrix} \left|KP(1-KP)^{-1}\right| < \frac{1}{|W_g \cdot V_n|} & \left|(1-KP)^{-1}\right| < \frac{1}{|W_g \cdot V_d|} \\ \left|K(1-KP)^{-1}\right| < \frac{1}{|W_u \cdot V_n|} & \left|K(1-KP)^{-1}\right| < \frac{1}{|W_u \cdot V_d|} \end{pmatrix} \tag{4.3}$$

Equation 4.3 can be written as:

$$\forall \omega \in \Re: \quad \begin{pmatrix} |T| < \frac{1}{|W_g \cdot V_n|} & |S| < \frac{1}{|W_g \cdot V_d|} \\ |R| < \frac{1}{|W_u \cdot V_n|} & |R| < \frac{1}{|W_u \cdot V_d|} \end{pmatrix} \tag{4.4}$$

4.4 Control goals and constraints

The controller should keep the air gap on a constant value. For achieving this, an optimal compromise between the control goals and constraints has to be found:

1. Stability

The closed loop system should be stable.
All transfers from equation (4.2) have to be checked on possible unstable poles. This means that unstable modes have to be reachable from **u** to guarantee the existence of a stabilising controller. The unstable modes also have to be observable from **y**.

2. Disturbance reduction

The influence of disturbances should be small.
From equation (4.2) follows that if we want to decrease the effect of the disturbance d on the output g, the transfer g/d (sensitivity) should be small in the frequency band where we want to keep the air gap g on a constant value. The disturbance reduction is large at low frequencies, because a small steady state error is desired.

The transfer g/d will therefore be small for a low frequency band. This frequency band should be chosen as large as possible to obtain robustness against disturbing rotation forces over a broad band, so that the final plant can stear the mirror very fast.

3. Sensor noise reduction

The noise introduced by the sensor should not effect the air gap.
The influence of the sensor noise on the output g should be small for the frequency band where the noise is most disturbing. Normally, the sensor noise appears often at high frequenies and therefore the transfer g/n (complementary sensitivity) should be small for high frequencies.

4. Avoidance of actuator saturation

The actuator should not become saturated.
There is assumed that for continuous operation, the actuator voltage u (=HcR in Figure 4.1) has to be in a range of: $-0.5V \leq HcR \leq 0.5V$
The maximum frequency of the actuator is assumed to be higher than the frequencies where the air gap is of interest.

5. Robustness

If the dynamics of the process changes the performance of the system should not be influenced.
The controller to be designed should be robust for the uncertainty block ΔP, modelling the additive perturbations. According to the small gain theorem the system of Figure 4.8 is asymptotic stable if:

$$\|M\Delta P\|_\infty < 1$$

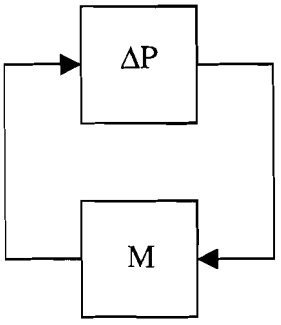

Figure 4.8: Small gain theorem

For additive perturbations holds: M = R

So, the system of Figure 4.8 is asymptotic stable if: $\|R\Delta P\|_\infty < 1$

If we assume that the controller stabilises the nominal plant P then the closed loop system is stable for all additive perturbations ΔP if:

$$\forall \omega \in \Re : |\Delta P(jw)| < \frac{1}{|R(jw)|} \tag{4.5}$$

From equation (4.4) we see that R is determined by the filters W_u,V_d and V_n. So by choosing these filters, we can combine the demands for actuator saturation and robust stability and performance.

4.5 Shaping and weighting filters

4.5.1 Shaping filters

• V_n
This filter represents the sensor noise. It is known that the sensor noise never rises above 5 mV. This results in: $V_n = 5$ mV ≅ - 46 dB.

• V_d
Shaping filter V_d is chosen constant and characterises the disturbance on the air gap height. The disturbance consists of disturbances due to the mentioned model perturbation ΔP and the disturbances of the air gap height, when the mirror is rotated. The last mentioned disturbance (100 mV) has been measured and written down in section 3.4 on page 27. This results first in: V_d = 100 mV ≅ -20 dB.

4.5.2 Weighting filters

• Wu
Weighting filter W_u weights the actuator signal u. This filter represents the model perturbation and should protect the actuator against saturation.

The amplitude of V_d was chosen at: -20 dB. Which corresponds the disturbances of the air gap height when the mirror is rotated. Then W_u is chosen to realise:

$$|W_u \cdot V_d| > |\Delta P|$$

Which is the same as equation (4.5).
After this the amplitude of W_u is adjusted together with the amplitude of V_d. This is done by minimizing the amplitude of W_u and by enlarging the amplitude of V_d, because $|W_u \cdot V_d|$ should be the same.
From simulations we can see whether this is allowed and does not saturate the actuator.

Finally, for the third order model weighting filter W_u and shaping filter V_d are chosen:

$$W_u = \frac{0.33472\,s^2 + 509.25\,s + 137860}{s^2 + 191.13\,s + 2015600}$$

$$V_d = 1$$

For the seventh order model weighting filter W_u and shaping filter V_d are chosen:

$$W_u = \frac{0.049734\ s^2 + 319.81\ s + 91085}{s^2 + 736.09\ s + 3220200}$$

$$V_d = 1$$

• Wg

Weighting filter W_g weights the actual air gap of the process. This filter is adjusted in bandwidth and amplitude to get a controller which compromises performance and robustness.

For the third order model weighting filter W_g is chosen:

$$W_g = \frac{0.06\ (s+10000)}{s+3}$$

For the seventh order model weighting filter W_g is chosen:

$$W_g = \frac{0.1\ (s+10000)}{s+5}$$

Figure 4.9 shows the Bode-plots of the shaping and weighting filters based on the 3rd order model.

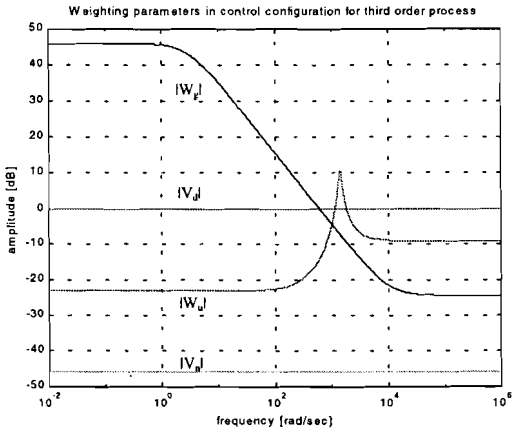

Figure 4.9: Shaping and weighting filters for 3rd order model of the process

Figure 4.10 shows the Bode-plots of the shaping and weighting filters based on the 7th order model .

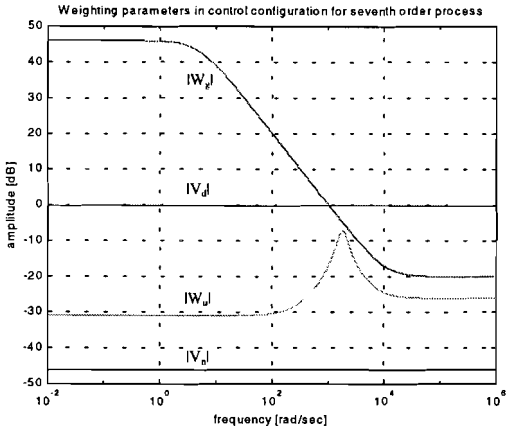

Figure 4.10: Shaping and weighting filters for 7th order model of the process

In Figure 4.11 and 4.12 the model perturbation and the shaping with W_u and V_d are plotted for respectively the 3rd order model and the 7th order model of the process.

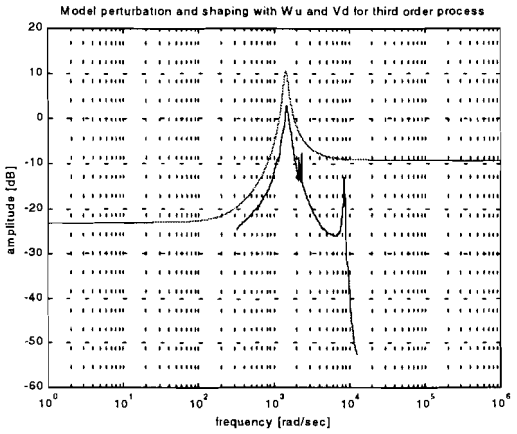

Figure 4.11: Model perturbation and |Wu·Vd| for 3rd order model of the process

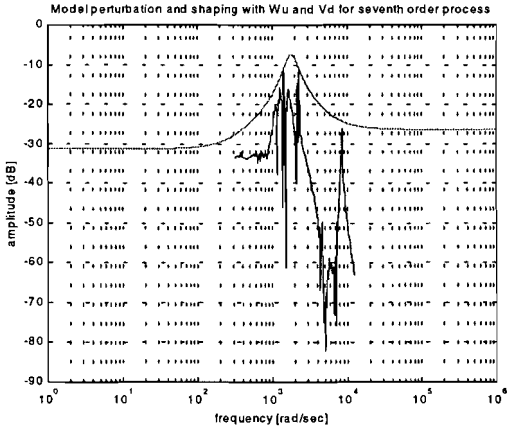

Figure 4.12: Model perturbation and |Wu·Vd| for 7th order model of the process

4.6 Weighting functions

The shaping and weighting filters result in the weightings for the sensitivity S, the complementary sensitivity T and the control sensitivity R. The two weightings for the control sensitivity R result in weightings for the complementary sensitivity T, because T=R · P. Where P is the magnitude of the process. So the process has one sensitivity bound and three complementary sensitivity bounds, see Figure 4.13 and 4.14. In these figures the intersection-point of the most relevant weightings for S and T should lay below the 0 dB-line.

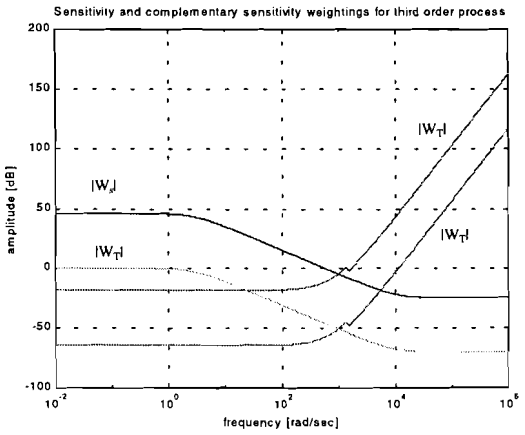

Figure 4.13: Weightings for S and T for 3rd order model of the process

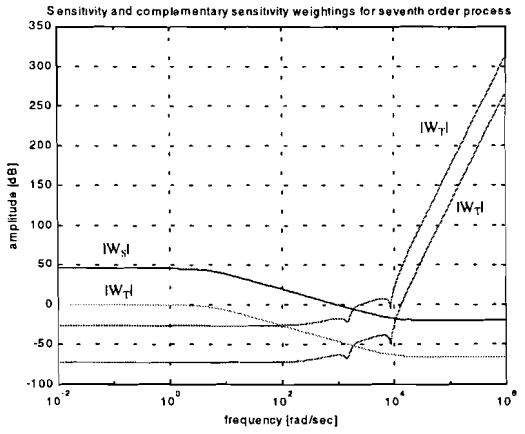

Figure 4.14: Weightings for S and T for 7th order model of the process

4.7 Closed loop evaluation

To prevent numerical problems in H_∞ controller design the pole of filter W_g is chosen near to the origin in stead of in the origin. Normally you would like to have a pole in the origin to get a zero steady state error. When the controller is calculated by the toolbox the nearest pole from the origin is shifted to the origin. So, finally the controller has one pole in the origin to get the wanted zero steady state error.

The MHC - Toolbox calculated the following gamma and controller for the approximated 3rd order model .

$$\gamma \approx 1.000035$$

The Bode-plot of the controller is shown in Figure 4.15. The upper plot shows the calculated controller by the toolbox. The lower plot is the adjusted controller with one pole in the origin.

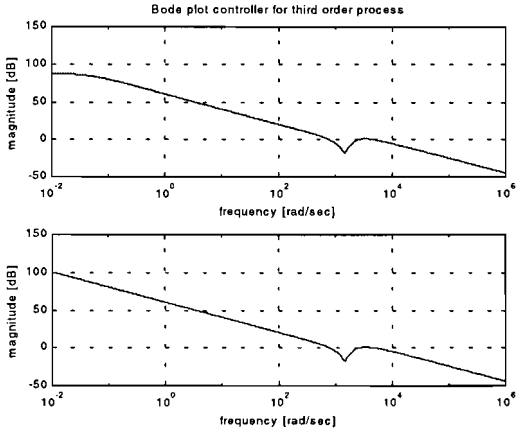

Figure 4.15: Bode-plot air gap controller for 3rd order model of the process

Because the MHC-Toolbox could not calculate a controller for the 7th order model there is switched to the LMI – Toolbox.
With the shaping and weighting filters the LMI - Toolbox calculated a gamma and a controller for the 7th order model .

$$\gamma \approx 1.000004$$

The Bode-plot of the controller is shown in Figure 4.16. The upper plot shows the calculated controller by the toolbox. The lower plot is the adjusted controller with one pole in the origin.

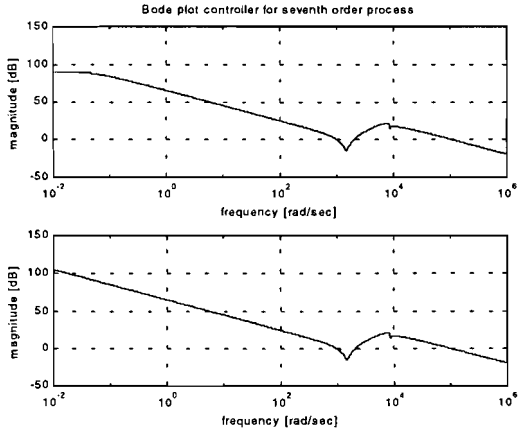

Figure 4.16: Bode-plot air gap controller for 7th order model of the process

The bandwidth of the air gap controller is limited around 210 Hz. Because at this frequency the resonance frequency, caused by the mass of the actuator and the pretension spring, causes the largest peak of the model perturbation ΔP which has to be attenuated.

The sensitivity is shaped by weighting filter $|W_s|^{-1}$. This filter is a combination of W_g and V_d. The complementary sensitivity is shaped by weighting filter $|W_T|^{-1}$. This filter is a combination of W_u,V_d and the magnitude of the process. Figure 4.17 and 4.18 shows the sensitivity S and complementary sensitivity T and their bounds when the pole of the controller is shifted to the origin.

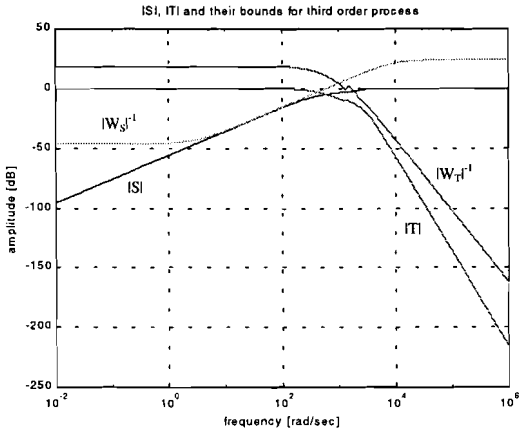

Figure 4.17: S and T with their bounds for 3rd order model of the process

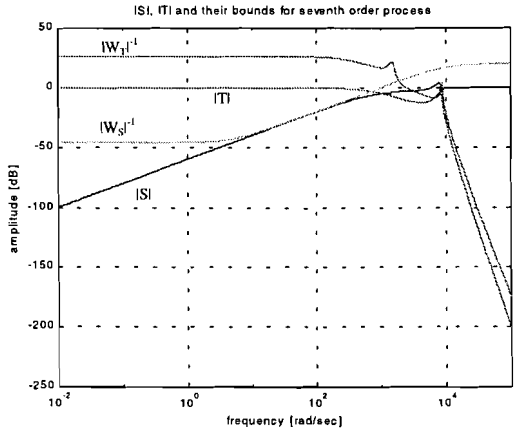

Figure 4.18: S and T with their bounds for 7th order model of the process

From Figure 4.17 and 4.18 we can conclude understanding items:

- Steady state error

The steady state error is determined by the magnitude of |S| at $\omega = 0$. In our case the steady state error is zero, because the pole of the controller is shifted to the origin.

- Bandwidth

The bandwidth is determined by choice of the cross-over frequency of |S|. The bandwidth is ≈ 600 rad/sec. for the approximated third order model and is ≈ 1000 rad/sec. for the seventh order model .

- Sensor noise reduction

The sensor noise reduction is determined by the magnitude of |T|. At high frequencies, higher than 600 rad/sec., the noise will be reduced by the controller based on the 3^{th} order model . The controller based on the 7^{th} order model reduces the noise for frequencies higher than 1000 rad/sec.

- Disturbance reduction

The disturbance reduction is determined by the magnitude of |S|. The controller based on the approximated 3^{rd} order model reduces disturbances with a frequency smaller than 600 rad/sec. Disturbances with a frequency smaller than 1000 rad/sec. are reduced by the controller based on the seventh order model . The disturbance reduction at high frequencies is determined by the value of |S| at high frequencies. The controller based on the 3^{rd} order model does not reduce disturbances from 600 rad/sec. and higher. Disturbances with a frequency higher than 1000 rad/sec. are not reduced anymore by the controller based on the seventh order model .

4.8 Simulations

In Simulink simulations are done to test the calculated air gap controller, see Figure 4.19. Process disturbances are added at the output of the process. The disturbance of the air gap height are caused by tilting the mirror in different directions. This disturbance can be modelled by a triangular wave or a sine wave.

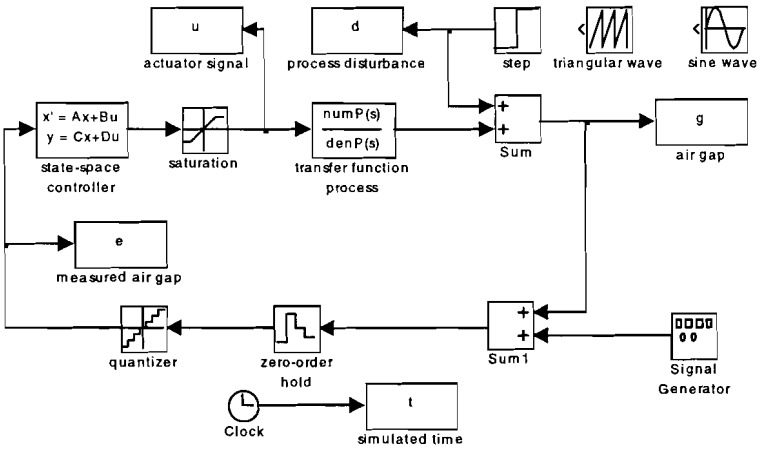

Figure 4.19: Block scheme of the air gap control system in Simulink

The controller is also tested with a step disturbance. This is done because a step disturbance gives a good indication if actuator saturation can be expected. The noise of the sensor is simulated by a random signal with a peak of 5 mV. In Figure 4.20 the simulated response of a step disturbance is given for the approximated 3rd order model. The amplitude of the disturbance is chosen 100 mV, because this is the maximum measured deviation of the air gap when the mirror is tilted in different directions. This deviation corresponds with 1.14 µm.

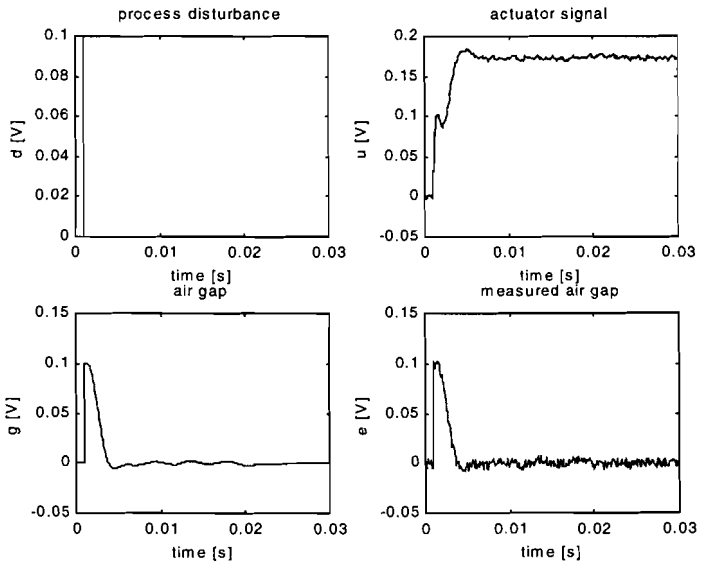

Figure 4.20: Simulated response of a step disturbance of 100 mV at 1 ms.

The actuator does not saturate and reaches a maximum value of almost 180 mV. After about 5 ms. the air gap becomes stable.
Figure 4.21 and 4.22 shows the simulated response of a triangular wave disturbance and a sine wave disturbance.

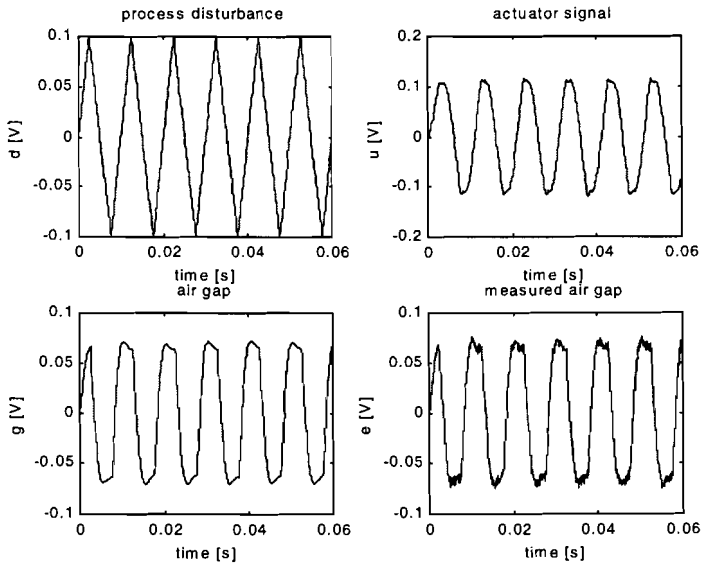

Figure 4.21: Simulated response of a triangular wave disturbance of 100 mV at 100 Hz

The triangular wave disturbance is reduced with a factor 1.5.

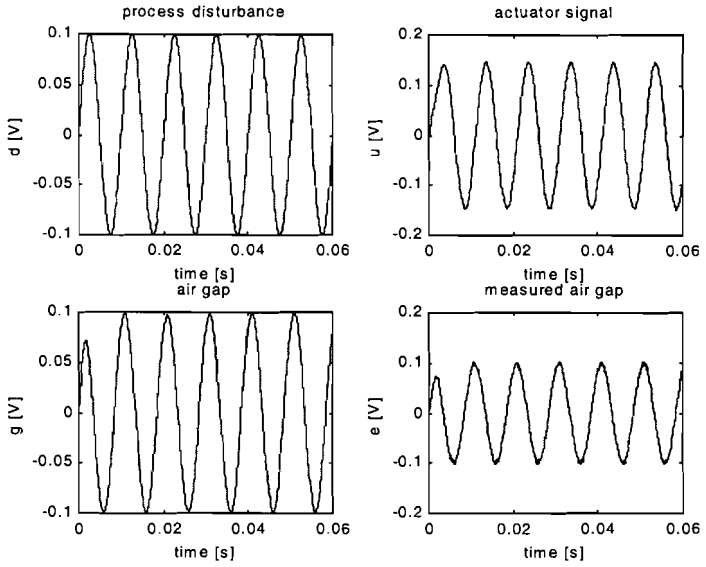

Figure 4.22: Simulated response of a sine wave disturbance of 100 mV at 100 Hz

The sine wave disturbance is not reduced anymore. So the bandwidth of the process is about 100 Hz.

The Figures 4.23, 4.24 and 4.25 shows the simulated response of the 7th order model of respectively a step disturbance, a triangular wave disturbance and a sine wave disturbance. In case of the triangular wave disturbance and the sine wave disturbance the frequency is chosen 150 Hz, because this is about the bandwidth of the process.

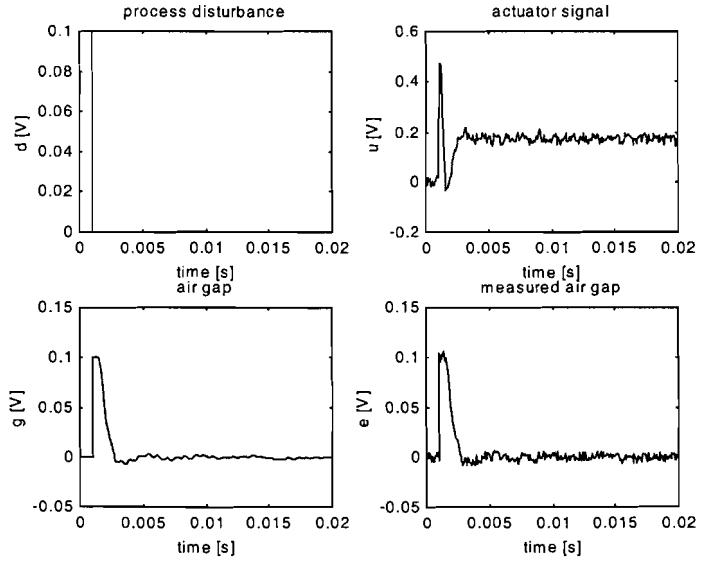

Figure 4.23: Simulated response of a step disturbance of 100 mV at 1ms

The actuator is not saturated and reaches a maximum value of almost 500 mV. After 5 ms the airgap becomes stable.

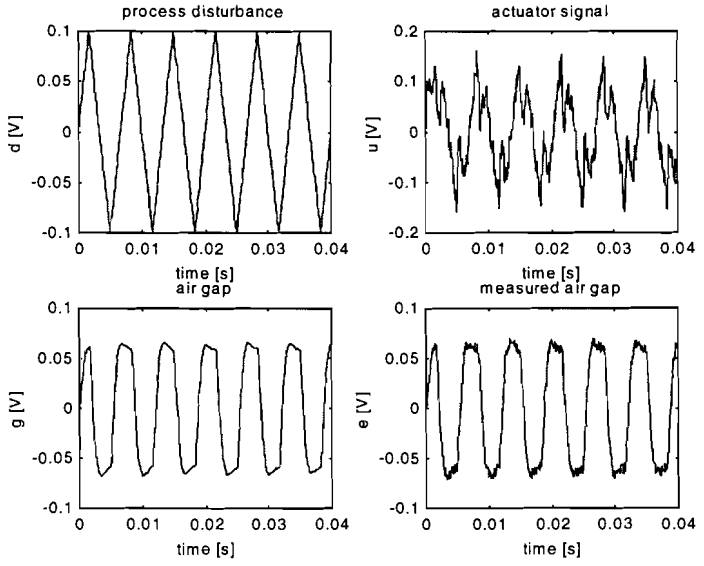

Figure 4.24: Simulated response of a triangular wave disturbance with an amplitude of 100 mV and 150 Hz.

The triangular wave disturbance is reduced with a factor 1.6.

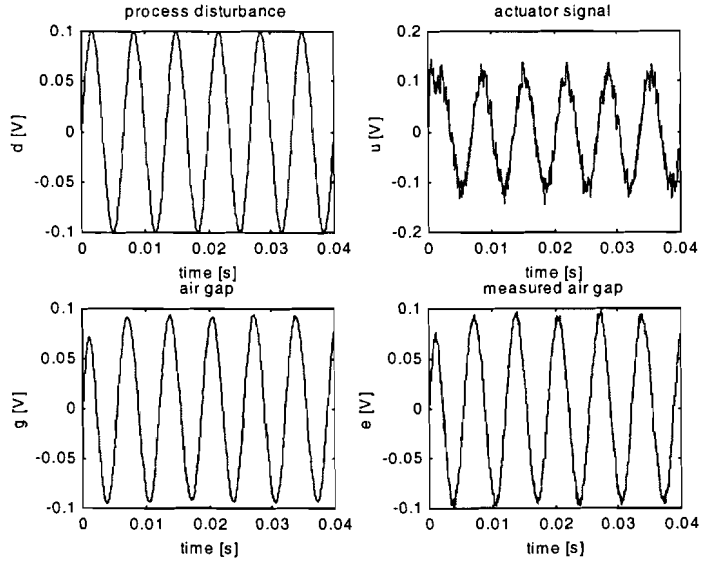

Figure 4.25: Simulated response of a sine wave disturbance with an amplitude of 100 mV and 150 Hz

The sine wave disturbance is nearly reduced anymore. From Figure 4.25 we can also conclude that the bandwidth of the process is 150 Hz.

4.9 Implementation

For testing the air gap controller on the real system, the controller must be implemented on a dSPACE system using the blockscheme of Figure 4.26. The integration method and sample frequency can be chosen in the "RTW Options" from the "Tools" dialog box in Simulink. The chosen integration method is: Euler, because this was the initialised method. The chosen sample frequency is: 13.000 Hz. This is the highest possible frequency to choose, a higher frequency resulted in a processor overload. It is advisable to choose a sample frequency of twenty times (if possible) the biggest frequency of the process and controller dynamics. The third order model has three poles from 210 Hz till 300 Hz. The seventh order model shows besides the poles of the third order model four poles at about 1500 Hz. The controller based on the third order model has poles/zeros till 600 Hz and the controller based on the seventh order model has poles/zeros till 1400 Hz. The implementation starts by choosing "RTW Build" from the "Tools" dialog box. Switches, see Figure 4.26, are added to start the controller with COCKPIT after the compilation.

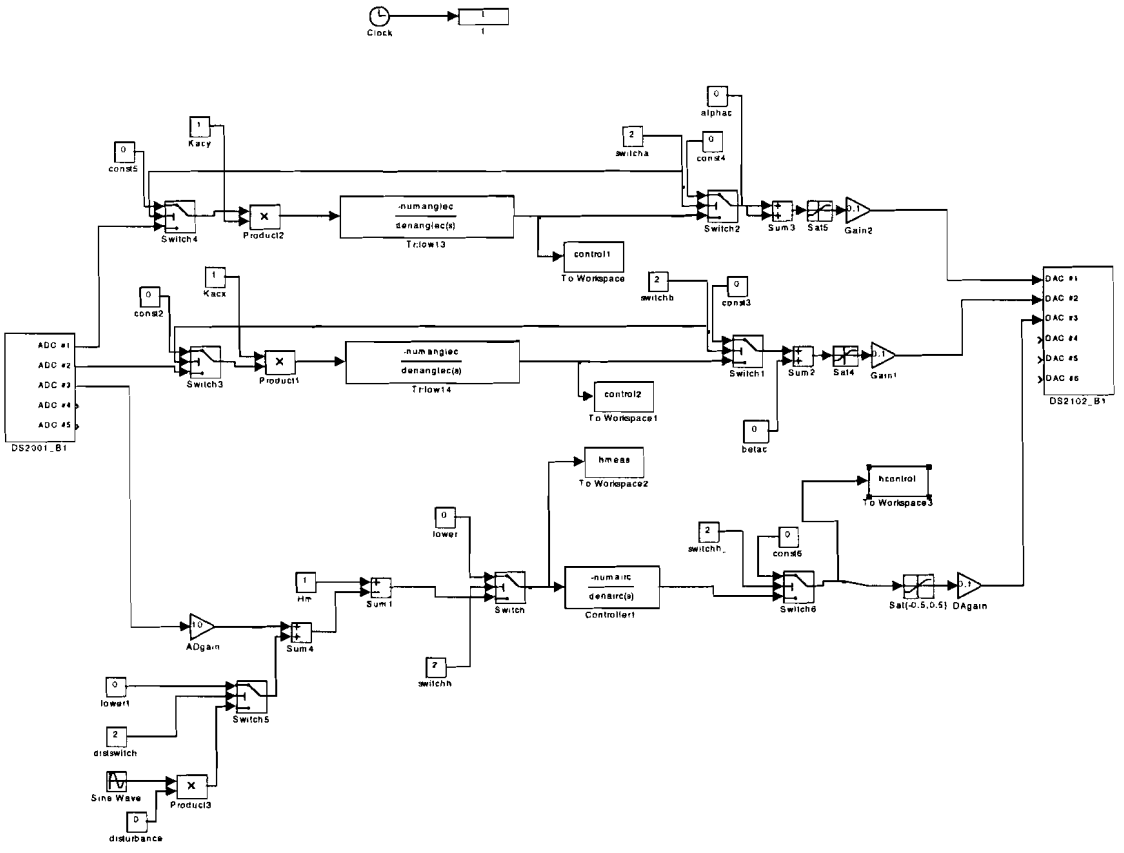

Figure 4.26: Block scheme used for implementation with dSPACE

First the controller based on the approximated third order model has been implemented. The controller has been tested by using an external sine wave disturbance of 100 Hz, with an amplitude of 100 mV. The results are given in Figure 4.27.

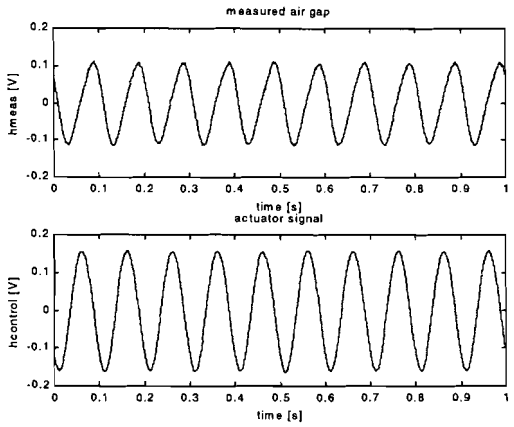

Figure 4.27: External sine wave disturbance

In Figure 4.27 can be seen that the measured air gap and the signals for the actuators are the same as the simulated signals from Figure 4.22 in Simulink.

The controller based on the seventh order model has also been implemented. This tenth order controller did not work. When we calculate a controller with the shaping and weighting filters based on the approximated third order model and we take the seventh order model, the dSPACE system can not handle this tenth controller either. So, we may conclude that a tenth order controller based on the seventh order model can not be implemented, because of the positions of the poles of the seventh order model at frequencies of 1500 Hz in combination with the sample frequency of 13000 Hz. If it would be possible to choose a greater sample frequency, a tenth order controller could be implemented probably.

To get a system with a larger bandwidth than 100 Hz, you can calculate a controller based on the third order model with weighting filters based on the seventh order model . In theory this is not allowed because $|\Delta P|$ would be bigger than $|W_u V_d|$. But in practice this worked. The controller calculated in this way is from the sixth order. The actuator signals are in this case much higher than for the controller based on the third order model with weighting filters based on the third order model .

5. H_∞ Angle controllers

For controlling the laser tracking system in the tracking mode, two angle controllers are designed. Each angle controller controls one angle of the mirror in its semi sphere. Both angle controllers are the same. There is again chosen for H_∞ controllers with the same reason as mentioned in chapter 4.

5.1 Transfer function of the process

For the two angles of the mirror in its semi sphere, α and β, we have the following transfer functions:

$$\alpha = \frac{r\sqrt{3}A(U_2 - U_3)}{as^3 + bs^2 + cs + d} \qquad \beta = \frac{r(-2U_1 + U_2 + U_3)A}{as^3 + bs^2 + cs + d}$$

U_1,U_2 and U_3 are the Laplace transforms of the input voltages to the actuators. For the meaning of the other parameters, see Appendix D: "Explanation of parameters."

To simplify the functions further the matrices T and $\tilde{T}$ are introduced:

$$T = \begin{pmatrix} 0 & \sqrt{3} & -\sqrt{3} \\ -2 & 1 & 1 \end{pmatrix} \qquad \tilde{T} = \begin{pmatrix} 0 & -\frac{1}{3} \\ \frac{1}{6}\sqrt{3} & \frac{1}{6} \\ -\frac{1}{6}\sqrt{3} & \frac{1}{6} \end{pmatrix}$$

such that with

$$\begin{pmatrix} U_\alpha \\ U_\beta \end{pmatrix} = T \begin{pmatrix} U_1 \\ U_2 \\ U_3 \end{pmatrix} \qquad \begin{pmatrix} U_1 \\ U_2 \\ U_3 \end{pmatrix} = \tilde{T} \begin{pmatrix} U_\alpha \\ U_\beta \end{pmatrix}$$

the transfer functions of the angles, can be written as:

$$\alpha = \frac{rAU_\alpha}{as^3 + bs^2 + cs + d} \qquad \beta = \frac{rU_\beta A}{as^3 + bs^2 + cs + d}$$

These transfer functions are the ones needed because the control inputs for the actuators of the real system are U_α and U_β. The transformation to U_1, U_2 and U_3 is done in hardware of the system.

In the real system the transformation from the inputs U_h (the voltage controlling the air gap, is the average of U_1,U_2 and U_3), U_α and U_β to U_1, U_2 and U_3, respectively, is done via:

$$\begin{pmatrix} U_1 \\ U_2 \\ U_3 \end{pmatrix} = \begin{pmatrix} \frac{1}{3} & 0 & -\frac{1}{3} \\ \frac{1}{3} & \frac{1}{6}\sqrt{3} & \frac{1}{6} \\ \frac{1}{3} & -\frac{1}{6}\sqrt{3} & \frac{1}{6} \end{pmatrix} \cdot \begin{pmatrix} U_h \\ U_\alpha \\ U_\beta \end{pmatrix}$$

Both the angle transfer functions are of third order.

The theoretical model of the transfer function, predicts three poles at: -17, -226 and -3757. [Linssen] verified the position of the three poles. The actual pole positions were found at: -60, -140 and -1775. These poles identify the process of the angle transfer function. In Figure 5.1 the Bode-plot of the angle transfer function is shown. Figure 5.2 shows the position of the poles.

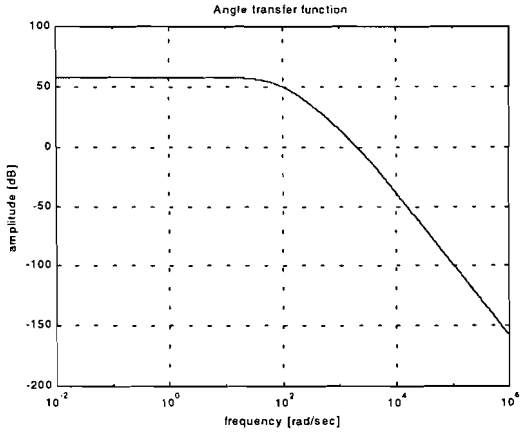

Figure 5.1: Bode-plot angle transfer function

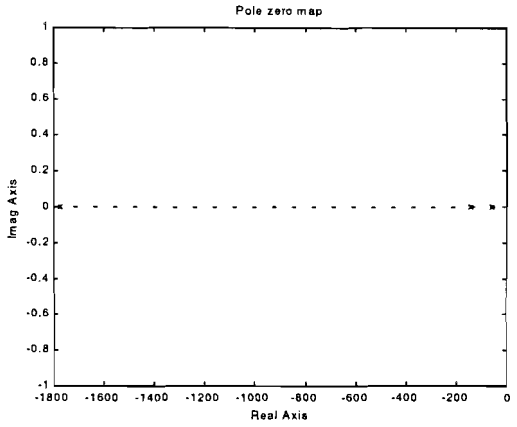

Figure 5.2: Pole-zero map of angle transfer function.

5.2 Block scheme with shaping and weighting filters

For H_∞ controlling a general block scheme is extended with shaping and weighting filters, see Figure 5.3.

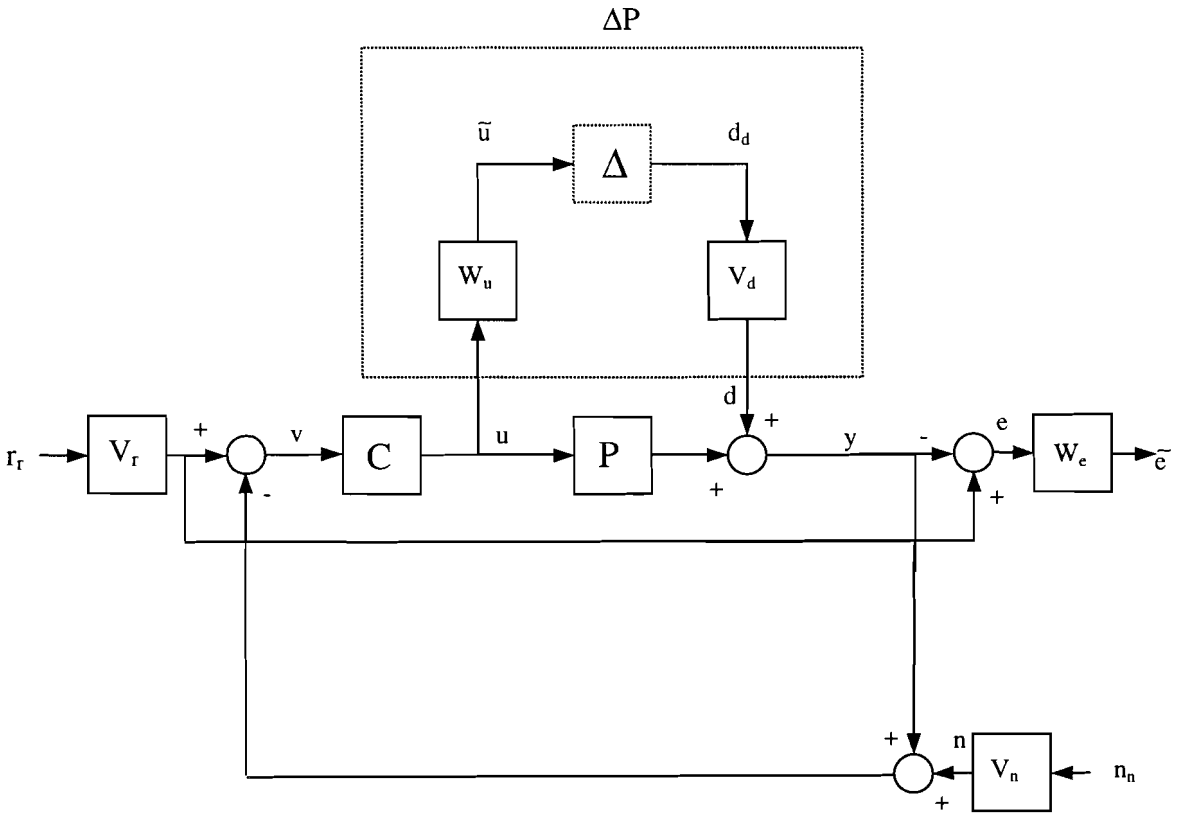

Figure 5.3: Block scheme with shaping and weighting filters

The block ΔP represents the additive model perturbation of the process.

ΔP is determined by:

Limited identification:	The poles predicted by the theoretical model are verified. This can not be done without an error.
Unmodelled dynamics:	The resonance frequencies caused by the actuators, at about 350 Hz are also not modelled in this case.
Time variance:	The dynamics of the process change in time due to, the influence of change in air pressure or temperature.

The shaping filters

- V_n

This filter represents the sensor noise.

- V_d

Shaping filter V_d characterises the disturbance on the angles of the mirror.

- V_r

This filter represents the reference signal.

The weighting filters

- W_u

Weighting filter W_u weights the actuator signal u. This filter represents the model perturbation and should protect the actuator against saturation.

- W_e

Weighting filter W_e weights the error of the process.

The error is defined as:

$$e = reference - real\ output$$

$$e = r - y$$

5.3 The augmented plant

The block scheme of Figure 5.3 results in the following augmented plant:

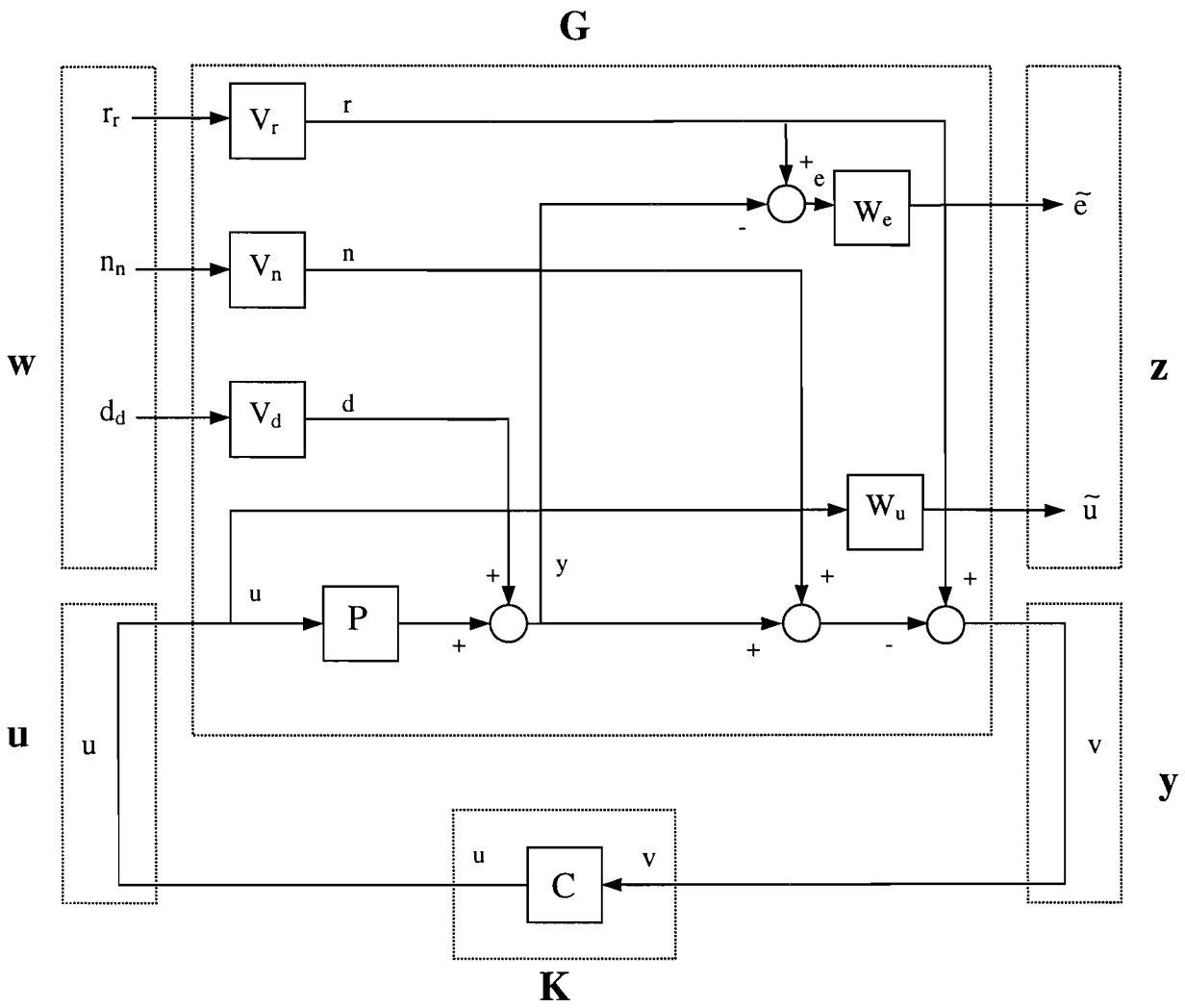

Figure 5.4: The augmented plant of the angle control system

From the augmented plant we can determine the following closed loop transfer matrix M:

$$M = \begin{pmatrix} \frac{\tilde{e}}{r_r} & \frac{\tilde{e}}{n_n} & \frac{\tilde{e}}{d_d} \\ \frac{\tilde{u}}{r_r} & \frac{\tilde{u}}{n_n} & \frac{\tilde{u}}{d_d} \end{pmatrix} = \begin{pmatrix} W_e \cdot \frac{I}{I+PK} \cdot V_r & W_e \cdot \frac{PK}{I+PK} \cdot V_n & W_e \cdot \frac{I}{I+PK} \cdot V_d \\ W_u \cdot \frac{K}{I+PK} \cdot V_r & W_u \cdot \frac{-K}{I+PK} \cdot V_n & W_u \cdot \frac{-K}{I+PK} \cdot V_d \end{pmatrix}$$

When it is realised to obtain:

$$\|M\|_\infty < \gamma \approx 1$$

Then it can be guaranteed that:

$\forall \omega \in \Re$:

$$\begin{pmatrix} \left|(1+KP)^{-1}\right| < \frac{1}{|W_e \cdot V_r|} & \left|KP(1+KP)^{-1}\right| < \frac{1}{|W_e \cdot V_n|} & \left|(1+KP)^{-1}\right| < \frac{1}{|W_e \cdot V_d|} \\ \left|-K(1+KP)^{-1}\right| < \frac{1}{|W_u \cdot V_r|} & \left|K(1+KP)^{-1}\right| < \frac{1}{|W_u \cdot V_n|} & \left|K(1+KP)^{-1}\right| < \frac{1}{|W_u \cdot V_d|} \end{pmatrix} \quad (5.1)$$

Equation 5.1 can be written as:

$$\forall \omega \in \Re : \quad \begin{pmatrix} |S| < \frac{1}{|W_e \cdot V_r|} & |T| < \frac{1}{|W_e \cdot V_n|} & |S| < \frac{1}{|W_e \cdot V_d|} \\ |R| < \frac{1}{|W_u \cdot V_r|} & |R| < \frac{1}{|W_u \cdot V_n|} & |R| < \frac{1}{|W_u \cdot V_d|} \end{pmatrix}$$

5.4 Control goals and constraints

In the tracking mode the laser tracking system should follow the retro-reflector even when the robot is moving at a high speed. To achieve this, an optimal trade off between the control goals and constraints has to be established.
For the angle controllers the same control goals and constraints hold as for the air gap controller. The angle controllers have even one extra goal:

Tracking
The aim is to let the output track the reference signal with a small error in a certain frequency band. If we want to decrease the tracking error, the transfer e/r should be small in the frequency band where we want to have a small tracking error. This corresponds to the disturbance reduction. So these aims could have been combined.

5.5 Shaping and weighting filters

It is known that the model perturbation is mainly caused by the unmodelled dynamics, which are discussed in the previous chapter. This means that resonance frequencies arise at 350 Hz. For this reason weighting filter W_u and shaping filter V_d looks like the filters W_u and V_d from chapter 4.

5.5.1 Shaping filters

- V_r

Shaping filter V_r is chosen first order, low frequent and chartacterises the reference signal.

$$V_r = \frac{4000}{s+2000}$$

• V_n

This filter represents the sensor noise. It is known that the sensor noise never rises above 5 mV. This results in: $V_n = 5$ mV $\cong$ - 46 dB.

• V_d

Shaping filter V_d is chosen constant and characterises the disturbances on the angles of the semi sphere. The disturbance is caused by the mentioned model perturbation ΔP. There is chosen: Vd = 1V $\cong$ 0 dB.

5.5.2 Weighting filters

• W_u

Weighting filter W_u weights the actuator signal u. Together with shaping filter V_d this filter represents the model perturbation.
To attenuate the resonance frequencies at 350 Hz, W_u shows a peak at about 350 Hz.

$$W_u = \frac{0.34342s^2 + 522.48s + 141440}{s^2 + 152.9s + 4031200}$$

• W_e

Weighting filter W_e weights the error of the process. This filter is adjusted in bandwith and amplitude to get a controller which compromises performance and robustness.

$$W_e = \frac{0.04(s + 10000)}{s + 2}$$

Figure 5.5 shows the Bode-plots of the chosen shaping and weighting filters.

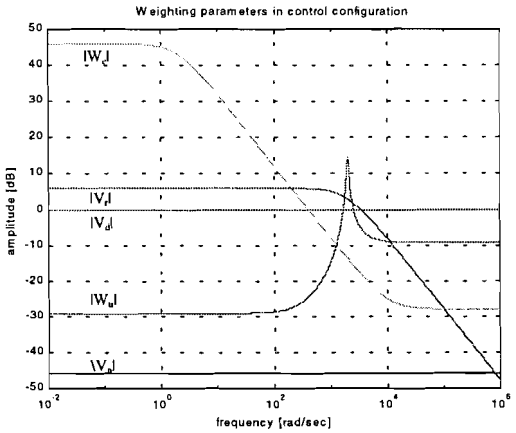

Figure 5.5: Shaping and weighting filters

5.6 Weighting functions

The shaping and weighting filters result in this case in two weightings for the sensitivity S, one weighting for the complementary sensitivity T and three weightings for the control sensitivity R. The weightings for the control sensitivity result again in weightings for the complementary sensitivity. In Figure 5.6 can be seen that the intersection-point of the most relevanted weighting for S and T lays below the 0 dB-line.

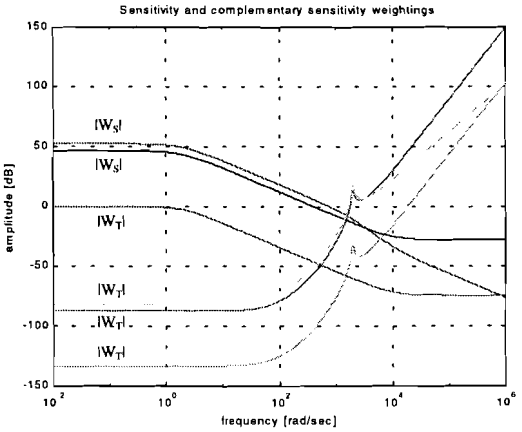

Figure 5.6: Weightings for S and T

5.7 Closed loop evaluation

The pole of filter W_e is chosen near to the origin in stead of in the origin to prevent numerical problems during H_∞ controller design. When the controller is calculated with the LMI-Toolbox the nearest pole from the origin is shifted to the origin. So, also this controller has one pole in the origin to get a zero steady state error.

The LMI-Toolbox calculated the following gamma and controller:

$$\gamma \approx 1.000022$$

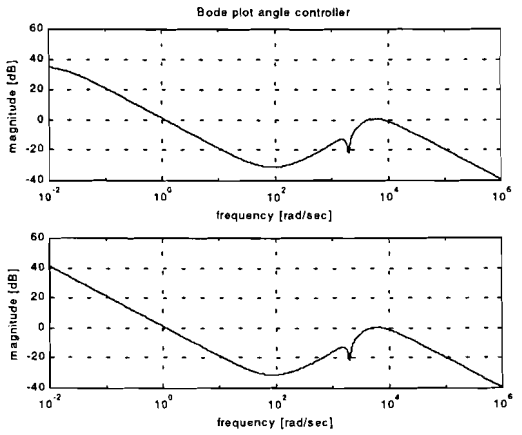

Figure 5.7: Bode-plot angle controller

The upper plot shows the calculated controller with the LMI-Toolbox. The lower plot is the adjusted controller with one pole in the origin.

The sensitivity is shaped by weighting filter $|W_S|^{-1}$. This filter is a combination of W_e and V_r. The complementary sentivity is shaped by weighting filter $|W_T|^{-1}$. This filter is a combination of W_u, V_r and the magnitude of the process. Figure 5.8 shows the sensitivity S and complementary sensitivity T and their bounds. The bandwidth is about 150 Hz.

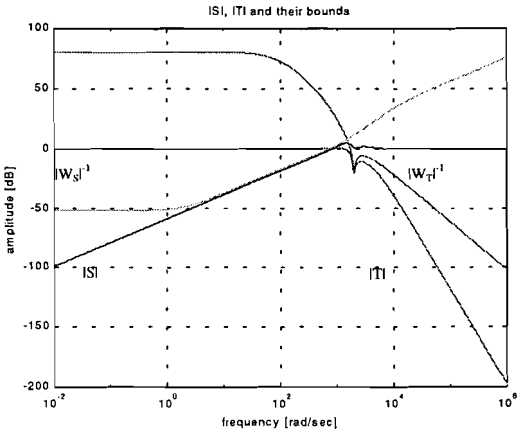

Figure 5.8: Sensitivity S and complementary sensitivity T with their bounds

5.8 Simulations

To see if the angle controller is able to track a reference signal, the angle controller is tested in Simulink, see Figure 5.9. A sine wave of 10 Hz is chosen as reference signal.

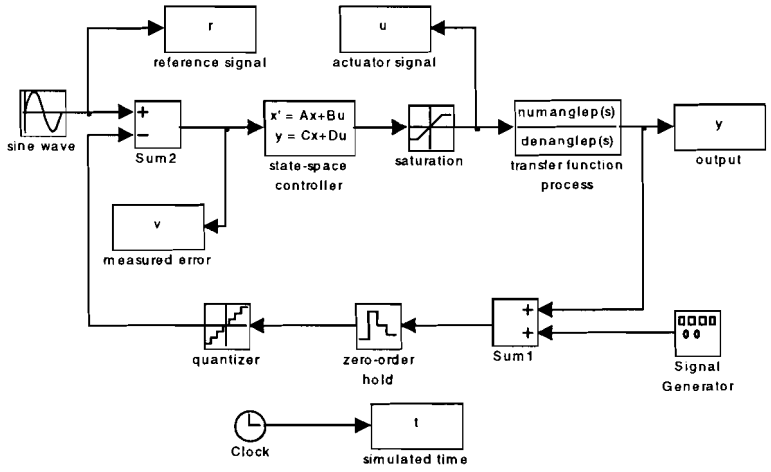

Figure 5.9: Block scheme of the angle control system in Simulink

The sensor resolution is simulated by noise with a maximum amplitude of 1 mV. The quantisation step is chosen equal to 20/2^16. The results of the simulations are given in Figure 5.10.

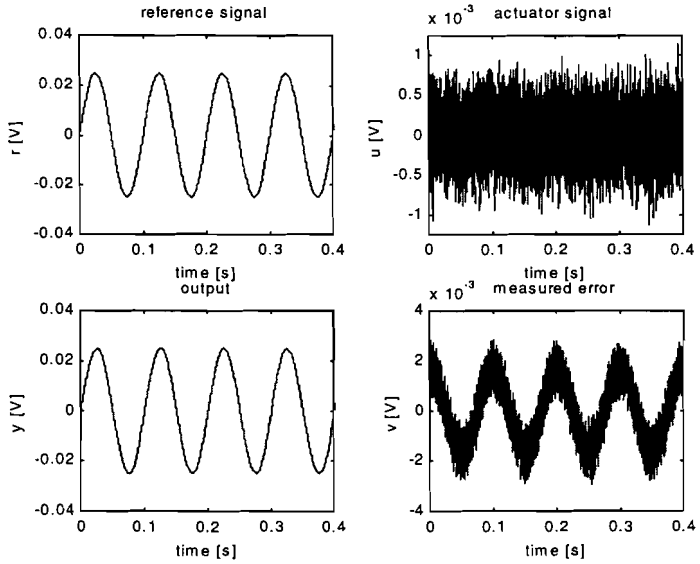

Figure 5.10: Simulation results angle controller

5.9 Implementation

For testing the angle controller on the real system the two angle controllers are implemented on the earlier mentioned dSPACE system by using the blockscheme of Figure 4.26 from Chapter 4. In the test setup the retro-reflector is attached to a wheel on the shaft of a motor. The motor turns the retro-reflector around with a frequency of 1.6 Hz. This means that we have a sine excitation in the x- and y-direction. Some results of the implementation are given in Figure 5.11 and Figure 5.12. In Figure 5.11 the x- and y-errors on the PSD are shown together with the control signals from the angle controllers.

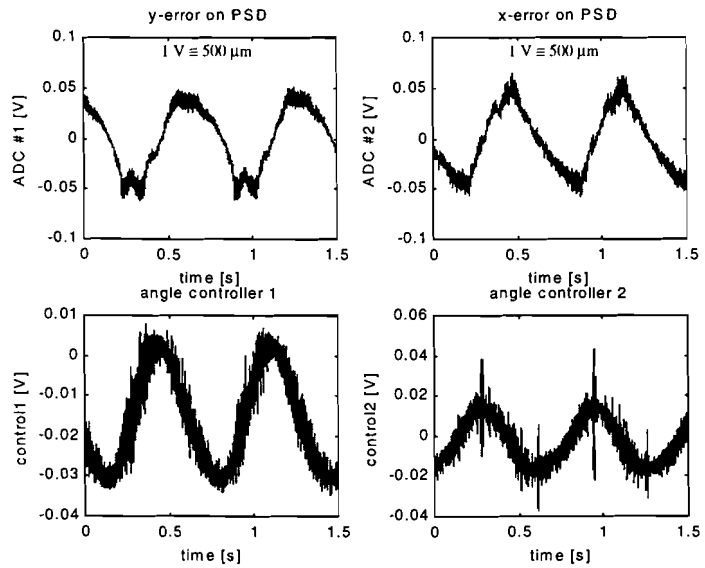

Figure 5.11: Implementation results angle controllers

The motor with servo amplifier has trouble turning around the weigth of the retro-reflector. These fast variations result in peaks of the control signals for the actuators.

In Figure 5.12 the air gap variation and the control signal from the air gap controller are given.

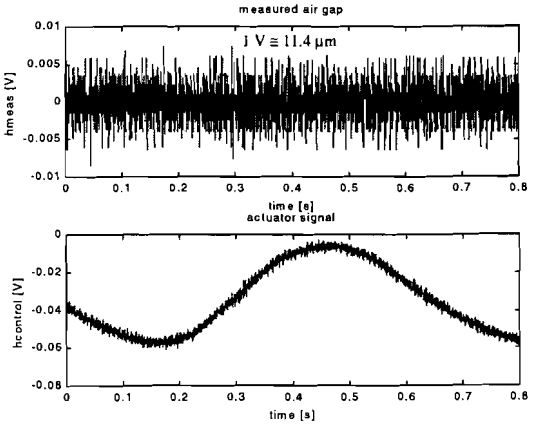

Figure 5.12: Implementation results air gap controller

6. Conclusions and recommendations

- **Accuracy analysis**

The accuracy analysis is done in a two-dimensional space. From the accuracy analysis it may be concluded that the inaccuracies caused by several kinds of displacements causes acceptable deviations of the length the laser beam travels and the angle of the mirror.

During the analysis we assumed that the sensors were ideal. It would be advisable to extend the analysis by taking in account that the sensors are not ideal.

To get a better sight on the total accuracy of the system it can be recommended to extend the analysis to a three-dimensional space.

From all external influences the temperature is the most important one. Measurements should be done to get more information about the temperature drift of the electronic components.

From the accuracy analysis may finally be concluded that α_l, the angle between the nominal position of the mirror and the incoming laser beam on the mirror, should be chosen between 40° and 60°.

- **H_∞ control**

For controlling the laser tracking system there is chosen for H_∞ controllers. With this controller it is possible to define and quantify the control aims very clearly by weighting the relatively. When using this controller, one has to make a trade off between robustness and performance.

To guarantee the accuracy of the laser tracking system it is important to take care for a constant air gap of the semi-sphere in its bearing seat. The air gap should be kept on a constant value for a bandwidth wider than the disturbing effects of mirror rotations.

To prevent numerical problems during the calculations of the controller in H_∞ controller design, the pole of the weighting filter which take care for a integrative action is chosen near to the origin in stead of in the origin. When the controller is calculated this pole is shifted to the origin to get the wanted integrator, which take care for a zero steady-state error.

Two controllers have been designed for controlling the air gap. One controller is based on a reduced third order model of the process. The other controller is based on the seventh order model of the process. The controller based on the reduced model is calculated in the MHC-Toolbox. Because the MHC-Toolbox could not calculate a controller based on the seventh order model there is chosen to calculate the controller for the seventh order model by using the LMI-Toolbox.

In the LMI-Toolbox the calculated controller with the MHC-Toolbox for the reduced model is checked. The results for the reduced model in the LMI-Toolbox were the same as in the MHC-Toolbox.

The air gap transfer function contains resonance frequencies at about 350 Hz. These resonance frequencies are not modelled and have to be attenuated. From measurements we can conclude that these resonance frequencies are caused by the actuators because these are not influenced by air gap variations. It would be very hard to model the resonance frequencies. Besides that would it be more possible to move the resonance frequency at about 210 Hz to a higher frequency. This can be realised by increasing the spring constant of the pretension springs. This resonance frequency is namely a combination of the actuator-mass and the spring constant.

During the implementation of the air gap controller based on the third order model there were no complications. The controller worked like the simulations went out. By implementing the tenth order controller, based on the seventh order model , it became clear that the dSPACE-system could not handle this controller. Maybe when it would be possible to choose a greater sample frequency this controller could be implemented on the real system.

The controller based on the third order model results in a bandwidth of the controlled system of 100 Hz. This is a double bandwidth according to an earlier developed PID-controller. To get a larger bandwidth than 100 Hz it is possible to calculate a controller based on the third order model with shaping and weighting filters based on the seventh order model . This controller results in a bandwidth of the controlled system of 150 Hz.

For controlling the laser tracking system in the tracking mode, two angle controllers have been developed. Because the unmodelled dynamics are independent of air gap variations and caused by the actuators these dynamics are taken for the model perturbation for the angle controllers. For this reason the shaping and weighting filters are basically the same as for the air gap controller. The angle controllers have even one extra filter, a shaping filter for the reference signal.

Appendix A: Explanations of used symbols in computations

Explanation of generally used symbols in computations

SYMBOL	DESCRIPTION
Xc	X-coordinate of retro-reflector
Yc	Y-coordinate of retro-reflector
Xs	X-coordinate of the incoming laser beam on the retro-reflector
Ys	Y-coordinate of the incoming laser beam on the retro-reflector
r	Distance from the mirror's center to the retro-reflector's centre
φ	Angle of the position of the retro-reflector's centre in ideal situation
l	Distance from laser to mirror in ideal situation
α_s	Angle of the mirror measured from the nominal position
α_l	Angle between nominal position of the mirror and the incoming laser beam on the mirror
α_c	Angle of the retro-reflector
α_{ci}	Angle of the incoming laser beam on the retro-reflector
$\Delta\alpha_s$	Change of the angle of the mirror, caused by a possible error (e.g. air gap height change)
L_1	Total distance of the laser beam in the ideal situation
L_2	Total distance of the laser beam by any displacement
B	Distance between incoming laser beam and reflected laser beam (position from PSD's center)

Explanation of used symbols in computation: "Effect of a side slip of the semi sphere."

SYMBOL	DESCRIPTION
δ	Side slip
δ'	Effect of a side slip in the Y-direction

Explanation of used symbols in computation: "An air gap variation of the semi sphere in its bearing seat."

SYMBOL	DESCRIPTION
δ	Air gap change
δ'	Effect of an air gap change in the Y-direction

Explanation of used symbols in computation: "Wrong alignment of the PSD."

SYMBOL	DESCRIPTION
δ	Distance of the wrong alignment of the PSD
l_1	Distance of the laser beam from the mirror to the retro-reflector
l_2	Distance of the laser beam inside the retro-reflector
l_3	Distance of the laser beam from the retro-reflector to the mirror
l_4	Distance of the laser beam from the mirror to the laser

Explanation of used symbols in computation: "The deflected laser beam does not point at the center of the mirror."

SYMBOL	DESCRIPTION
δ	Incorrect angle of the laser beam by pointing at the center of the mirror
δ'	Distance of the laser beam from the centre of the mirror at a distance of 1 m
l'	Distance of the laser beam from the laser to the mirror
r'	Distance of the laser beam from the mirror to the retro-reflector

Appendix B: The proof of the independence of the measuring distance on the length the laser beam travels.

$$D = 2\left(-\delta' + \sqrt{Xc^2 + (Yc - \delta')^2} - r\right)$$

$$= 2\left(-\delta' + \sqrt{(r\cos\varphi)^2 + (r\sin\varphi - \delta')^2} - r\right)$$

$$\approx 2\left(-\delta' + \sqrt{(r\cos\varphi)^2 + (r\sin\varphi)^2 - 2\delta' r\sin\varphi} - r\right)$$

$$= 2\left(-\delta' + r\sqrt{\cos^2\varphi + \sin^2\varphi - \frac{2\delta'\sin\varphi}{r}} - r\right)$$

$$= 2\left(-\delta' + r\sqrt{1 - \frac{2\delta'\sin\varphi}{r}} - r\right)$$

$$\approx 2\left(-\delta' + r\left(1 - \frac{\delta'\sin\varphi}{r}\right) - r\right)$$

$$= -2\delta'(1 + \sin\varphi)$$

Appendix C: The path of the laser beam at the retro-reflector when the alignment of the PSD is wrong

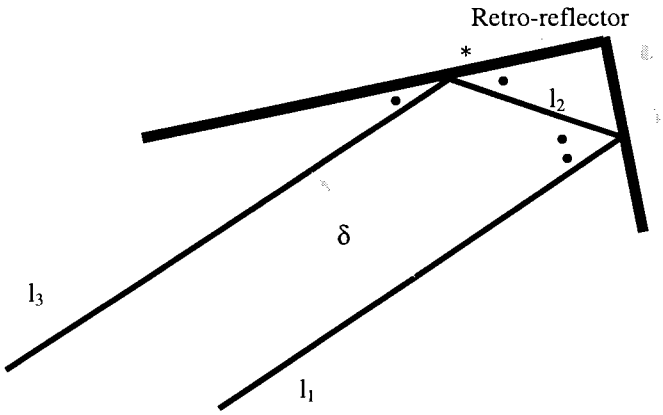

• = α_{ci} * = α_c

$$\sin\alpha_{ci} = \frac{d}{l_2}$$

$$\sin 2\alpha_{ci} = \frac{\delta}{l_2}$$

$$d = l_2 \sin\alpha_{ci} = \frac{\delta \sin\alpha_{ci}}{\sin 2\alpha_{ci}}$$

Appendix D: Explanation of parameters

$$a = L(2j + 3r^2 m)$$

$$b = 3r^2 DL + 3r^2 mR + 2jR$$

$$c = 3r^2 (DR + kL + A^2)$$

$$d = 3r^2 kR$$

Parameter	Value	Description
A	3.16 [kg·m·s^{-2}·A^{-1}]	Actuator constant depending on coil radius, number of windings and magnitude of the magnetic field
D	0 [N·s·m^{-1}]	Damping
j	10.6·10^{-8} [kg·m^2]	Moment of inertia around the centre of the mirror's surface in xy-plane
L	10^{-3} [H]	Induction of the coil
m	9.5 [kg]	Mass of coil
r	7·10^{-3} [m]	Distance from center of mirror to connection of actuator string
R	4 [Ω]	Resistance of coil

Bibliography

[SCH 86] Schellekens, P.H.J.
ABSOLUTE MEETNAUWKEURIGHEID VAN TECHNISCHE LASER INTERFEROMETERS.
Eindhoven: University of Technology, 1986.
Thesis

[SCH 89] Schüßler, H.H.
DOKUMENTATION GENAUIGKEIT VON LASER INTERFEROMETER- SYSTEMEN.
Düsseldorf: VDI-Verlag GmbH, 1989.
V.D.I.-Berichte No. 750.

[HAI 92] Haitjema, H.
LASER INTERFEROMETER CALIBRATION IN THE NETHERLANDS
In: Calibration and Testing of Laser Interferometers
Collection of papers and printed information of participants in the EUROMET-Workshop. Berlin, 11-12 March 1992.
Ed. by H. Kunzmann et al.
Braunschweig: Physikalisch-Technische Bundesanstalt, 1992. P. 75-85.

[LEI 97] Leigh-Lancaster, C.J. and B. Shirinzadeh, Y.L. Koh
DEVELOPMENT OF A LASER TRACKING SYSTEM.
In: Mechatronics and Machine vision in practice. 4 th Annual Conference on Mechatronics and Machine Vision in Practice. Toowoomba (Australia), 23-25 September 1997. Ed. by B. Werner et al.
London: IEEE, 1997. P. 163-168.

[VIN 94] Vincze, M. and J.P. Prenninger, H. Gander
A LASER TRACKING SYSTEM TO MEASURE POSITION AND ORIENTATION OF ROBOT END EFFECTORS UNDER MOTION.
The International Journal of Robotics Research, Vol. 13 (1994) No. 4, P. 305-314.

[DAM 98] Damen, A.A.H. and Weiland, S.
ROBUST CONTROL
Measurement and Control Group, Department of Electrical Engineering, Eindhoven University of Technology, 1998.

[FAL 94] Falkus, H.M. and Damen, A.A.H.
MULTIVARIABLE H-INFINITY CONTROL DESIGN TOOLBOX
Faculty of Electrical Engineering, Eindhoven: University of Technology, 1994.

[LOO 97] Looymans, R.L.M.
H∞-CONTROL OF THE AIR GAP OF A LASER DEFLECTING SYSTEM
Measurement and Control Group, Faculty of Electrical Engineering, M. Sc. Thesis, Eindhoven: University of Technology, 1997.

[LIN 98] Linssen, S.
SENSOR AND CONTROL DEVELOPMENT OF A LASER TRACKING SYSTEM
Measurement and Control Group, Faculty of Electrical Engineering, M. Sc. Thesis, Eindhoven: University of Technology, 1998.